Microwave Solid-State Active Devices

George I. Haddad, *Life Fellow, IEEE,* and Robert J. Trew, *Fellow, IEEE*

Invited Paper

***Abstract*—Solid-state devices have had a major impact on the development of microwave and millimeter-wave systems. Starting with development work dating back to the 1940s, a variety of two- and three-terminal device structures have been proposed, fabricated, and found their way into commercial and military applications. These devices have resulted in the realization of numerous systems that would not otherwise be possible. The device development effort has been closely linked to advances in semiconductor materials growth and processing technology. Many of the advanced device concepts can only be implemented with the advent of advanced materials growth technology, such as molecular-beam epitaxy, and fine-line lithography techniques, such as electron-beam lithography. Advanced materials technology has also provided the ability to fabricate heterostructures that permit the advantages of multiple material layers to be optimized for device applications. High-performance diodes and transistors are now available for use from UHF into the millimeter-wave spectrum, approaching terahertz frequencies. The development, operating principles, and state-of-the-art of various diode and transistor structures are reviewed.**

***Index Terms*—Active device, diode, electron beam, heterostructure, lithography, MBE, microwave, molecular-beam epitaxy, semiconductor, solid-state device, transistor.**

I. Introduction

ALTHOUGH the concept of a semiconductor device was considered by Braun as early as 1874 [1], successful demonstration occurred with the invention of the bipolar transistor by Bardeen, Brattain, and Shockley in 1948 [2], [3]. Although the transistor had high-frequency potential, the first transistors with RF gain and noise-figure performance sufficient for practical application at microwave frequencies were not produced until 17 years later. In 1965, the first practical transistor was fabricated using Ge and had a noise figure of 6 dB in L-band. Since then, device performance has rapidly improved and a variety of solid-state diodes and transistors are now extensively used in all modern systems. Early attempts to make use of semiconductor materials for active devices were focused upon attempts to translate vacuum tube concepts into a semiconductor environment. Both two-terminal diode and three-terminal transistor structures are possible and were developed. Early three-terminal work was directed toward fabricating a solid-state equivalent of the vacuum triode. This work dates back to patents by Lilienfeld in 1930 [4] and 1933 [5] for the concept of a solid-state field-effect transistor, and to the early work of Stuetzer [6], [7] in 1950 and Shockley in 1952 [8], the first serious attempts to fabricate the device. The early work was hindered by poor semiconductor material quality and technology limitations that prevented the realization of short gatelengths required for good dc and RF performance. The performance of the Ge devices was limited by low bandgap that resulted in high leakage currents and poor thermal performance. There was a search for semiconductors with improved properties and Si soon replaced Ge as the semiconductor material of choice. The development of III–V compound semiconductors such as GaAs, InP, and related ternary compounds permitted microwave and millimeter-wave devices with excellent noise and power performance to be developed. Progress was rapid due to advances in both fabrication technology and materials science and, by the early 1970s, high-performance GaAs MESFETs with good RF performance at X-band were developed and became commercially available. Today, RF performance of field-effect transistors extends well into the millimeter-wave region, and frequency response greater than 300 GHz has been reported for InP-based compound semiconductor high electron-mobility transistor (HEMT) devices.

Active diodes have also had a significant impact upon the development of microwave systems, and the first practical solid-state sources were constructed using IMPATT and Gunn devices. The IMPATT diode dates back to the early work of Shockley [9], who proposed the development of negative resistance from transit-time effects, and Read [10] who proposed a complex multilayered diode structure that utilized a combination of avalanche and transit-time effects to generate a phase shift greater than 90° between the RF voltage and current. The diode, when placed in a resonant cavity, was capable of oscillation. The complex diode structure proposed by Read was difficult to realize and, although these devices could produce microwave oscillations [11], it was shown about the same time that microwave oscillations could also be obtained from a simple p-n junction diode device [12], which was much easier to fabricate. The technology rapidly advanced and, in the 1970s, the development of techniques for semiconductor crystal growth such as molecular-beam epitaxy (MBE) permitted both optimized p-n junction and read-type IMPATT diode structures to be realized. These devices were capable of excellent RF power and efficiency performance well into the millimeter-wave spectrum [13]. About the same time,

Manuscript received November 5, 2001.

G. I. Haddad is with the Electrical Engineering and Computer Science Department, University of Michigan at Ann Arbor, Ann Arbor, MI 48109 USA.

R. J. Trew is with the Electrical and Computer Engineering Department, Virginia Polytechnic Institute and State University, Blacksburg, VA 24061 USA.

Publisher Item Identifier S 0018-9480(02)01981-6.

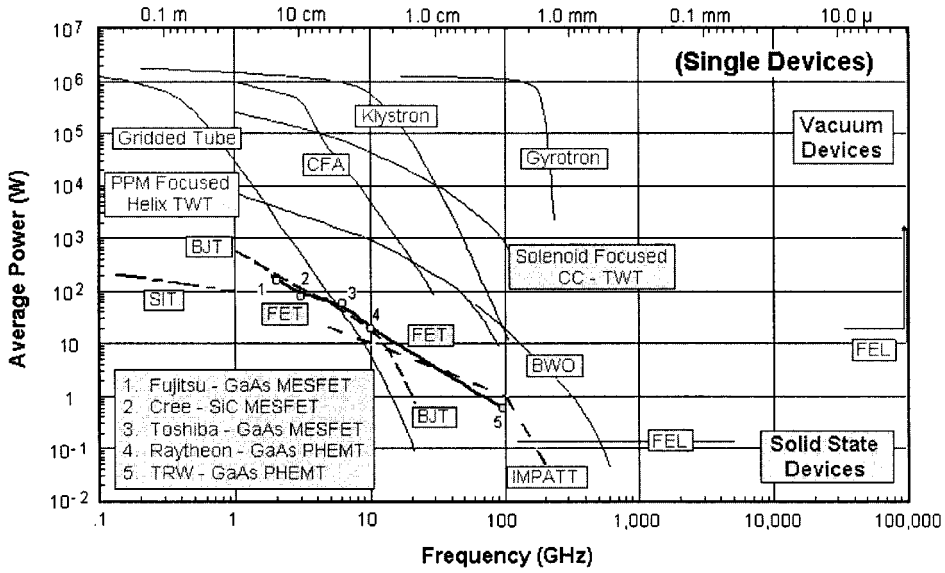

Fig. 1. Average RF output power versus frequency for various electronic devices (courtesy of Naval Research Laboratory; V. L. Granatstein, P. K. Oarker, and C. M. Armstrong, "Scanning the technology: Vacuum electronics at the dawn of the twenty-first century," *Proc. IEEE (Special Issue)*, pp. 702–716, vol. 87, May 1999).

another type of two-terminal active device was developed that also proved to be very useful in microwave systems. Following the observation of negative resistance effects in GaAs crystals by Gunn in 1963 [14], a transferred electron effect [15], [16] was demonstrated to be due to the complex conduction band of certain III–V semiconductors and the effect could be used to fabricate active devices for use in microwave sources and amplifiers. These devices were generally termed Gunn or transferred electron devices (TEDs) and they found wide use in microwave and millimeter-wave systems, particularly for local-oscillator applications due to a combination of wide tuning bandwidth and moderate noise performance. Although the first Gunn devices were fabricated in GaAs, InP is also used to fabricate devices due to improved high-frequency performance [17]. In general, the performance of the two-terminal devices at high frequency was superior to that from transistors and many practical microwave and millimeter-wave systems were designed using active diode sources.

The current state-of-the-art of microwave solid-state devices designed for RF power applications is compared to that for microwave tubes in Fig. 1. As indicated, solid-state devices produce RF power levels less than about 100 W and operate with reasonable RF output power to frequencies of about 100 GHz. The RF performance status shown in Fig. 1 is for single device operation, and does not necessarily represent a true comparison of the RF output power capability of a system. Power-combining and phased-array technology permit the outputs of many solid-state devices to be combined, thereby producing significantly improved RF output power, and solid-state systems can, in practice, compete in terms of RF output power with tube-based systems. Combining technology can raise microwave RF output power into the kilowatt range, at least through X-band and into X-band, and theoretically to much higher power levels. However, such multidevice concepts are increasingly difficult to apply as operating frequency increases and cannot extend the upper frequency limit beyond the present state-of-the-art. Operation at frequencies above X-band and up to 100 GHz with RF output power in the hundreds of watts or kilowatt range will require new semiconductor materials and/or device concepts.

II. Semiconductor Materials

The dc and RF performance capability of solid-state devices is fundamentally dependent upon the properties of the semiconductor material from which they are fabricated, and the success of microwave solid-state devices has been due in large part to advances in the quality of semiconductor bulk and epitaxial materials. There has been a continued improvement in the quality of semiconductor materials dating back to the first demonstrations of these devices. Bulk growth has primarily focused upon technologies to produce semiconductor wafers for use as substrates for the growth of device quality epitaxial layers, and device fabrication generally occurs in the epitaxial material. The focus of bulk technology is to produce substrate wafers with a low density of defects and uniform and controlled impurity density. Both low- and high-resistivity substrates are necessary, depending upon the type of device to be fabricated. The low-resistivity substrates are generally used for vertical devices, such as diodes and bipolar transistors, where the current flow must pass through the substrate material. High-resistivity substrates are used for surface-oriented devices, such as field-effect transistors, where the current flow is parallel to the substrate. For the latter devices, good dc and RF performance generally require that current flow be confined to the epitaxial layer and blocked from the substrate.

A variety of technologies for growth of semiconductor epitaxial layers have been developed dating back to the first demonstration of solid-state devices. The first epitaxial layers were based upon liquid-phase epitaxial (LPE) growth technology where a molten semiconductor is passed over a substrate and, as it cools, it produces thin semiconductor layers that are lattice matched to the substrate. By including controlled densi-

ties of impurities in the molten material, relatively thin layers of doped p- or n-type material are formed. The process requires high temperature for the liquid flow process and it is difficult to produce thin layers with uniform thickness and precise and spatially uniform impurity concentration due to diffusion effects. The process is, however, low cost and was widely used for early devices. Chemical vapor phase technology also developed about the same time. In the chemical vapor deposition (CVD) process, hot gases are passed over a substrate where they cool and produce epitaxial growth. This process also requires high temperature and, like the LPE process, is not capable of producing thin layers with uniform thickness and well-controlled impurity concentration. Advanced epitaxial technology for advanced device fabrication developed in the 1970s with the development of MBE. The process requires chambers operated at high vacuum and involves heating of various material element sources to produce atomic fluxes, which are directed to a substrate. As the atomic fluxes land upon the substrate, they form epitaxial growth with very precise growth characteristics. Since the growth is at relatively low temperature, diffusion effects are minimized and very thin layers with precise thickness and impurity control are produced. Also, by including multiple sources, it is possible to fabricate binary, ternary, or quaternary compounds. Complex layer structures with atomic layer control can be fabricated and this has proven instrumental in the development of device structures with optimized performance. This ability led to the development of heterostructure devices, such as HEMTs and quantum-well structures, which are now widely used for advanced microwave and millimeter-wave devices. Although MBE technology enabled the development of complex device structures, the technology was limited to relatively small substrate wafer size and high throughput was difficult to achieve. The technology is also costly. These factors limit the use of the technology for high-production applications. Attention was directed toward development of vapor-phase epitaxy where larger substrates could be used. It was discovered that the use of organic catalysts could lower the temperature of the growth process and results competitive with MBE could be achieved. The process is called organic–metallic chemical vapor deposition (OM-CVD) and developed rapidly. Today, OM-CVD and MBE technologies are competitive and produce essentially equivalent device structures. Both technologies can produce a variety of complex heterojunction and multilayered structures suitable for advanced microwave and millimeter-wave devices.

The dc and RF performance of a solid-state device is determined by a combination of mechanical, thermal, and electrical properties of the semiconductor material from which it is fabricated. Much of the focus of research in materials has been to identify and synthesize semiconductor materials with desired and optimized properties. A summary of some of the semiconductor material properties most important to electronic device performance is listed in Table I for several semiconductors. Desirable material properties include a large energy gap, a low value of dielectric constant, high thermal conductivity, and high critical electric field for breakdown. Wide energy bandgap generally translates into an ability to support high internal electric fields before electronic breakdown occurs, and also provides for improved radiation resistance. Most semiconductor device fabrication has been in Si, GaAs, and InP and related compounds and virtually all devices commercially available are fabricated from these materials. Recently, there has been interest in the development of devices from wide-bandgap materials such as SiC and GaN. These materials have energy bandgaps about two to three times those in the conventional semiconductors. The dielectric constant is an indication of the capacitive loading of a device and affects the terminal impedance. Generally, a low value for the dielectric constant is desired, and this permits a semiconductor device to be larger in area for a given impedance. Increased area permits larger RF currents and higher RF power to be generated. The thermal conductance of the material is extremely important since this parameter indicates the ease with which dissipated power can be extracted from the device. Poor thermal conductivity results in device operation at elevated temperature with degraded performance. Compound semiconductors such as GaAs and InP are, in general, poor thermal conductors and this introduces complexity in device design for devices designed to operate at high power. Diamond and SiC are excellent thermal conductors and are often used for heat-sink applications. Finally, the critical electric field for electronic breakdown should be high. This parameter is an indication of the strength of the electric fields that can be supported internally in the device before breakdown. High electric fields permit large terminal RF voltages to be supported, and this is necessary for the generation of high RF power. One of the attractive features of the wide-bandgap materials is a high value for the critical field, which is typically an order of magnitude greater than for conventional semiconductors.

TABLE I
MATERIAL PROPERTIES FOR SEVERAL SEMICONDUCTORS

Material	E_g *(eV)*	ε_r	κ *(W/°K-cm)*	E_c *(V/cm)*
Si	1.12	11.9	1.5	3×10^5
GaAs	1.43	12.5	0.54	4×10^5
InP	1.34	12.4	0.67	4.5×10^5
3C-SiC	2.3	9.7	4	1.8×10^6
4H-SiC	3.2	10.0	4	3.5×10^6
6H-SiC	2.86	10.0	4	3.8×10^6
GaN	3.4	9.5	1.3	2×10^6
Diamond	5.6	5.5	20-30	5×10^6

Basically, a current is defined as the movement of charge and expressed as the product between the charge density and transport velocity. Therefore, the dc and RF currents that flow through a device are directly dependent upon the charge carrier velocity versus electric-field transport characteristics of the semiconductor material. Generally, for high currents and high frequency, high charge carrier mobility and high saturation velocity are desirable. A comparison of the electron velocity–electric (v–E) field characteristics for several semiconductors is shown in Fig. 2.

The v–E characteristic is described in terms of charge carrier mobility μ_n, (units of $\text{cm}^2/\text{V}\cdot\text{s}$) defined from the slope of the v–E characteristic at low electric field, and the saturated velocity v_s (units of cm/s), defined when the carrier velocity ob-

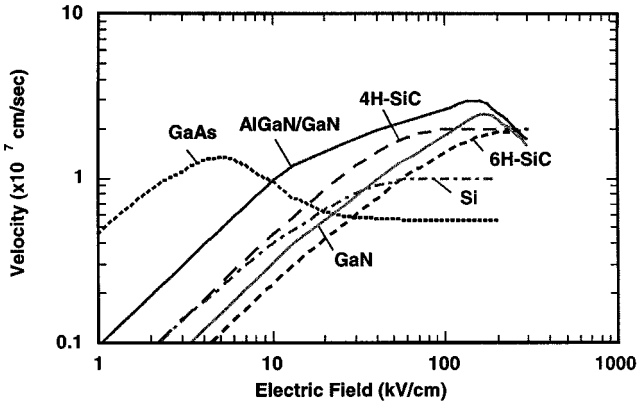

Fig. 2. Electron velocity versus electric field characteristics for several semiconductors ($N_d = 10^{17}$ cm^{-3}).

tains a constant field-independent magnitude, generally at high electric field. The high value for electron mobility of GaAs (typically $\mu_n \sim 5000$ cm^2/V $\cdot$ s) is the main reason that field-effect transistors fabricated from this material have such excellent low-noise and high-frequency performance. The v–E characteristics shown in Fig. 2 are for transport through semiconductors doped at $N_d = 10^{17}$ cm^{-3}, which is a typical impurity concentration used in device fabrication.

The magnitude of electric field that produces saturated charge carrier velocity is also important since the device must be able to develop the saturation field to obtain maximum RF performance and high-frequency operation. In general, low saturation fields are desirable, and this relates to the magnitude of the mobility. Hole transport is also important for devices, such as diodes and bipolar transistors, which use p-n junctions. Hole transport, however, tends to be significantly lower than for electrons, and hole mobilities for all semiconductors are generally low. This can result in high values for series and contact resistance, which limit device performance. For this reason, majority carrier devices such as field-effect transistors where channel currents can be limited to electronic flow have been favored for microwave and millimeter-wave applications. Heterojunction bipolar transistors (HBTs), however, have also been developed and, by design, optimization where the effects of low mobility p-type regions are minimized, excellent RF performance is obtained.

III. Two-Terminal Devices

Two-terminal devices were the first solid-state devices to be employed for generation and amplification at microwave frequencies. Although they have been mostly replaced by three-terminal devices at microwave and lower millimeter-wave frequencies, they still hold record performance in terms of power generation capability, particularly at shorter millimeter and submillimeter wavelengths.

There are essentially several types of two-terminal devices that are suitable for power generation. These include Esaki tunnel diodes (TDs) [18], [19], resonant tunneling diodes (RTDs) [20], TEDs or Gunn-effect devices [14], [16], and transit-time devices utilizing various types of injection mechanisms including avalanche breakdown, tunneling, and barrier injection. These transit-time devices are generally known as IMPATTs [10], TUNNETTs [21], and BARITTs [22], [23]. All of these devices exhibit a negative differential resistance (NDR) property, although the basic mechanisms for generating the negative resistance are different. Such devices can be used either as reflection-type amplifiers or oscillators. Reflection-type amplifiers can be realized either by using a circulator to separate the input and output or by injection locking of the device operating as an oscillator. Here, we will mainly discuss the use of these devices as oscillators. An equivalent circuit for an oscillator utilizing a negative resistance device is shown in Fig. 3.

The admittance per unit area Y_D is given by

$$Y_D = -G_D + jB_D \tag{1}$$

and the total admittance

$$Y_d = -AY_D = -AG_D + jAB_D \tag{2}$$

where $A =$ the device area.

The device impedance is

$$Z_d = \frac{1}{Y_d} = -R_d - jX_d \tag{3}$$

where

$$R_d = \frac{G_D}{A(G_D^2 + B_D^2)} \tag{4}$$

and

$$X_d = \frac{B_D}{A(G_D^2 + B_D^2)}. \tag{5}$$

For the devices under consideration and at high operating frequencies, $B_D \gg G_D$ and (4) and (5) reduce to

$$R_d = \frac{G_D}{AB_D^2} \tag{6}$$

and

$$X_d = \frac{1}{AB_D}. \tag{7}$$

The oscillation condition is satisfied when $R_d = R_s + R_L$ and $X_d = X_L$. This results in

$$\omega_o L_L = \frac{1}{\omega_o C_d} \tag{8}$$

and

$$\omega_o = \frac{1}{\sqrt{L_L C_d}}$$

is the oscillation frequency.

The power generated by the device is given by

$$P_{\mathrm{RF(Gen.)}} = \frac{1}{2} V_{\mathrm{RF}}^2 A G_D \tag{9}$$

where $V_{\mathrm{RF}} =$ the magnitude of the RF voltage.

From (6) and the matching condition for oscillation, we have

$$\frac{G_D}{AB_D^2} = R_s + R_L. \tag{10}$$

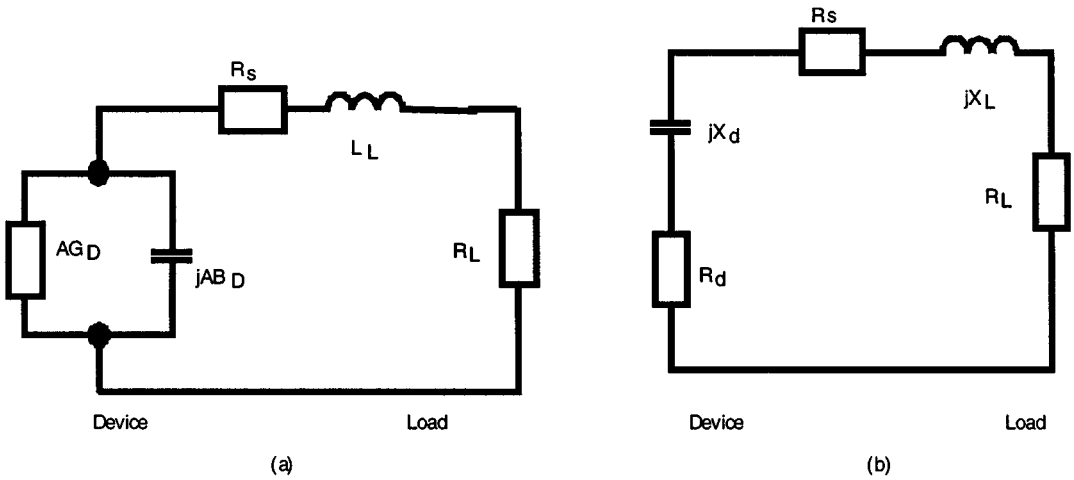

Fig. 3. Simplified equivalent circuit of an oscillator with a two-terminal device connected to a load.

Therefore,

$$A = \frac{G_D}{B_D^2(R_S + R_L)} \tag{11}$$

and

$$P_{\mathrm{RF(Gen.)}} = \frac{1}{2} V_{\mathrm{RF}}^2 \frac{G_D^2}{B_D^2(R_S + R_L)}. \tag{12}$$

The power delivered to the load R_L is given by

$$\begin{aligned} P_{\mathrm{RF}}(R_L) &= P_{\mathrm{RF}}(\mathrm{Gen.}) \frac{R_L}{(R_S + R_L)} \\ &= \frac{1}{2} V_{\mathrm{RF}}^2 \frac{G_D^2}{B_D^2 R_L \left(1 + \dfrac{R_S}{R_L}\right)^2}. \end{aligned} \tag{13}$$

It is, therefore, seen that knowledge of G_D and B_D for various operating parameters and device designs for a particular device is what is needed to estimate the power generation capability and efficiency as well as the device area.

These devices can be operated under pulsed conditions as well as continuous wave (CW). Therefore, there are two limitations for power generation capability. The first is electronic and the second is thermal. The electronic generation capability is limited by matching to the load resistance, including the series resistance of the device. The thermal limitation is determined by the thermal resistance of the device, which depends on various parameters, including area, heat sink, and layer structure. For additional details on fabrication technology and heat sinking, the reader should refer to [10].

IV. Two-Terminal Solid-State Negative-Resistance Devices

A. Tunneling Devices

In this category (which does not include TUNNETTs because transit-time effects are negligible), we include Esaki TDs and RTDs. They both exhibit negative-resistance in their I–V characteristic ranging from dc to very high frequencies. The electronic power output is mainly limited by the large capacitance of the device. Esaki TDs [18] were proposed in 1958 and were utilized in oscillators up to 100 GHz. However, the power output from these devices was very small compared to the other two-terminal devices and, therefore, are not in much use at this time. More recently, an RTD [20] was proposed that has a much better speed index (I/C), and can be tailored to optimize the important parameters through heterostructure engineering. We will, therefore, discuss the RTD here, keeping in mind that similar characteristics are obtained from TDs. In TDs, tunneling takes place between the conduction band and valence band of a heavily doped p^+–n^+ junction and, thus, is referred to as interband tunneling. However, in an RTD, tunneling takes place through the conduction bands of a double-barrier heterostructure, as shown in Fig. 4. The basic mechanism for the negative resistance property is also illustrated in this figure. As is well known, tunneling electrons maintain energy and must have available states to tunnel through. A typical diode structure and I–V characteristic are shown in Fig. 5. The structure shown in this figure utilizes AlAs barriers [25] and GaAs quantum wells. Other material systems [26]–[29] have also been employed and exhibit higher frequency performance.

In contrast to the other two-terminal devices, the negative resistance of an RTD persists over a very wide frequency range and extends to dc This presents problems relative to bias circuit oscillations and the bias circuit must be included in an estimate of power generation capability. Thus, the equivalent oscillator circuit is shown in Fig. 6.

In order to gain a better understanding of the power generation capability of this device, we will assume a linearized I–V characteristic, as shown in Fig. 7. Referring to this figure, we assume that the device is biased in the middle of the negative resistance region [i.e., $V_{\mathrm{DC}} = (1/2)(V_p + V_v)$ and $I_{\mathrm{DC}} = (A/2)(J_p + J_v)$]. Assuming that the RF voltage swing is limited to the negative resistance region, the maximum RF voltage swing will be

$$V_{\mathrm{RF}} = \frac{1}{2}(V_v - V_p). \tag{14}$$

The negative conductance per unit area G_D is given by

$$G_D = \frac{J_v - J_p}{V_v - V_p} \tag{15}$$

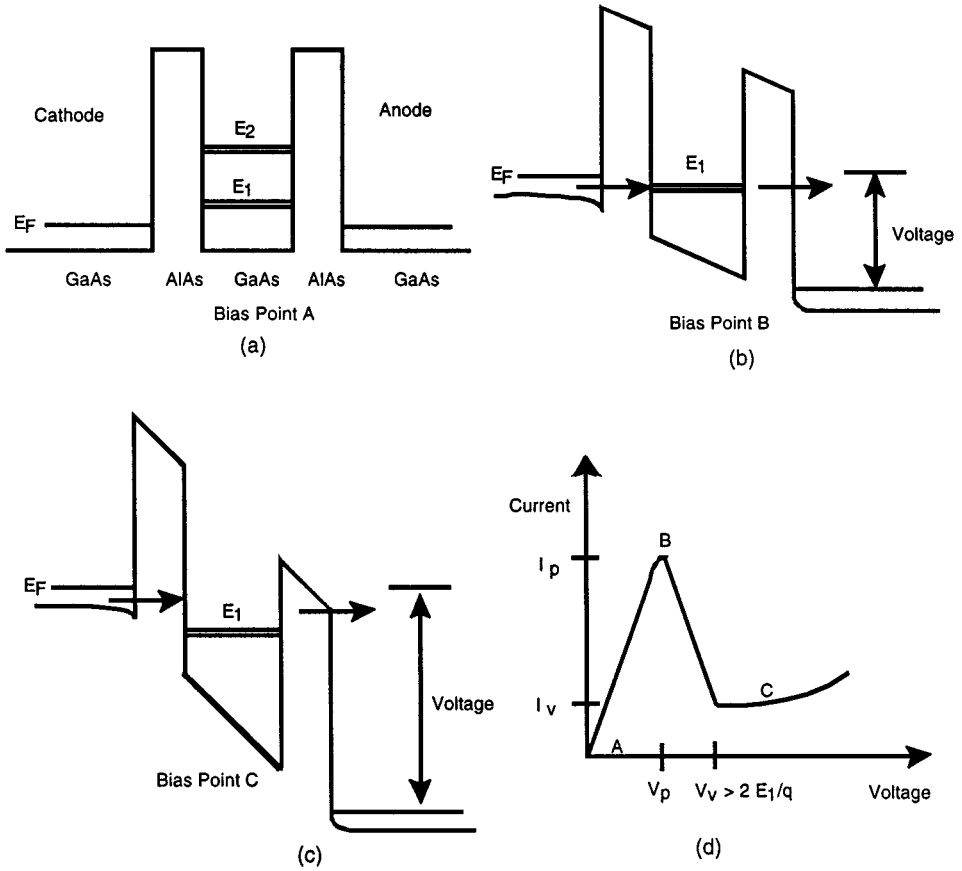

Fig. 4. (a)–(c) Bias-dependent band diagrams at the three bias points A, B, and C. (d) Current–voltage characteristic for a GaAs/AlAs double heterobarrier structure.

and the diode susceptance per unit area B_D is represented by

$$B_D = \omega C_D = \omega \frac{\varepsilon_s}{W} \tag{16}$$

where

C_D capacitance per unit area;
ε_S dielectric constant;
W depletion-layer width.

The diode area A and the RF power generated are obtained from (9), (11), and (13), and are given by

$$P_{\mathrm{RF(Gen)}} = \frac{1}{8} A (J_p - J_v)(V_v - V_p). \tag{17}$$

The dc to RF conversion efficiency η is given by

$$\eta = \frac{P_{\mathrm{RF}}}{P_{\mathrm{DC}}} = \frac{1}{2} \frac{\left(\frac{J_p}{J_v} - 1\right)\left(\frac{V_v}{V_p} - 1\right)}{\left(\frac{J_p}{J_v} + 1\right)\left(\frac{V_v}{V_p} + 1\right)}. \tag{18}$$

The circuit limited RF power is given by

$$P_{\mathrm{RF}}(R_L) = \frac{1}{8}\left(\frac{J_p}{\omega_o C_D}\right)^2 \left(1 - \frac{J_v}{J_p}\right)^2 \frac{R_L}{(R_L + R_S)^2}. \tag{19}$$

However, since the negative resistance in this device extends to dc, another limitation arises when bias circuit instabilities are to be avoided. This limitation is related to the bias circuit inductance [30], [31] and can be expressed as

$$L_S \leq \frac{AC_D}{A^2 G_D^2} = \frac{C_D}{A G_D^2} \tag{20}$$

and

$$A \leq \frac{C_D}{L_s G_D^2}. \tag{21}$$

In this case, the bias-circuit limited RF power is given by

$$P_{\mathrm{RF}}(\text{bias circuit limited}) = \frac{1}{8}(V_v - V_p)^3 \frac{1}{(J_p - J_v)} \left(\frac{C_D}{L_S}\right). \tag{22}$$

This presents a severe limitation on the power generation capability of these devices for finite L_S since $(V_v - V_p)$ in these devices is very small.

For the experimental device shown in Fig. 3, we can estimate $(V_v - V_p) = 0.5$ V, $J_p = 40$ kA/cm^2, $J_p/J_v = 3.5$, and $W = 70$ nm. The output power from such a device can then be estimated [21] for both limits, and the results are shown in Fig. 8.

Fig. 9 summarizes the best experimental results obtained to date from RTDs in several material systems [25], [27]–[29]. It is seen from this data that an oscillation frequency of 712 GHz was obtained and is the highest fundamental frequency achieved

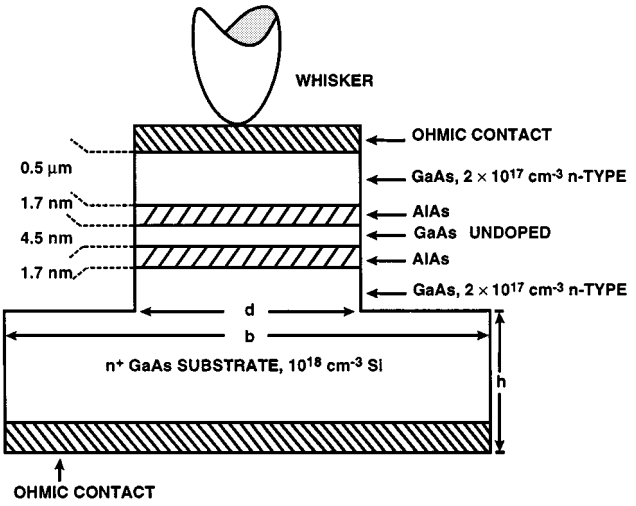

(a)

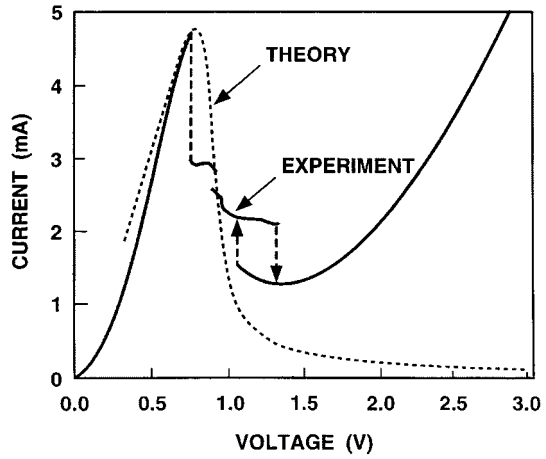

(b)

Fig. 5. (a) Cross section of a mesa-type AlAs/GaAs/AlAsRTD. (b) Measured and theoretical current–voltage characteristics [25].

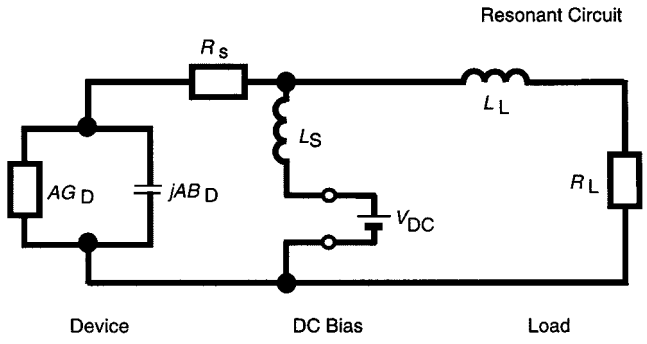

Fig. 6. Simplified equivalent circuit of an oscillator with an RTD connected to a bias circuit and a load.

to date from a solid-state source. However, the power level was approximately 0.3 μW.

B. TEDs

These devices utilize the basic transport properties in bulk materials to generate the negative resistance. They are unipolar devices where no p–n junction is required as compared to the other two-terminal devices presented. These devices exhibit low-noise performance and are well suited for local oscillator applications. They require materials with a particular band structure, which is found in several semiconductor materials, particularly III–V compounds. In order for a material to be suitable in these applications, it must possess the following

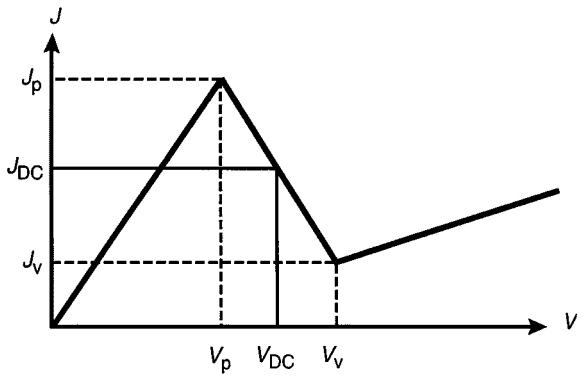

Fig. 7. Linearized current–voltage characteristic of an RTD.

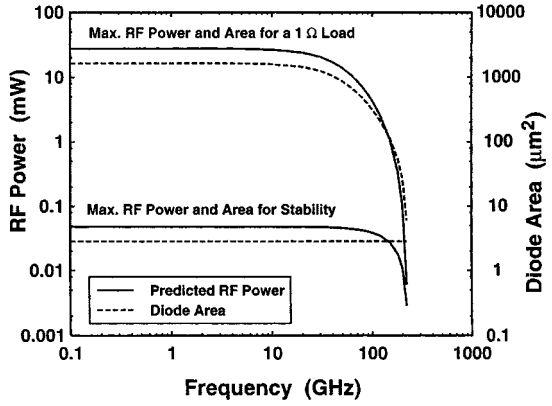

Fig. 8. Top curves: predicted RF output power and diode area for matching into $R_L = 1\ \Omega$. Bottom curves: predicted RF output power and diode area for obtaining stability with $L_S = 0.1$ nH. Linearized current–voltage characteristics for the diode of Fig. 7 are assumed.

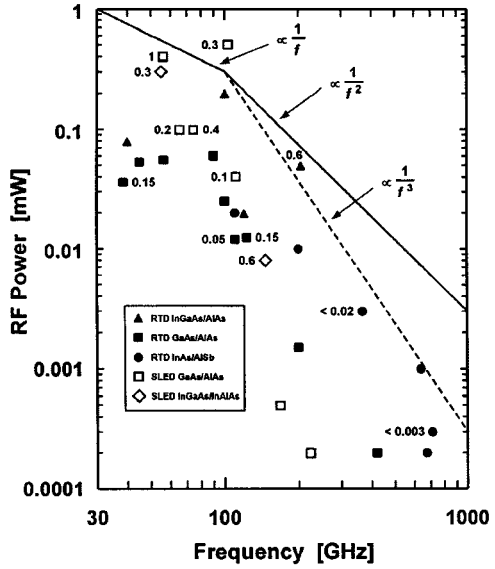

Fig. 9. State-of-the-art RF power levels from RTDs in the frequency range of 30–1000 GHz.

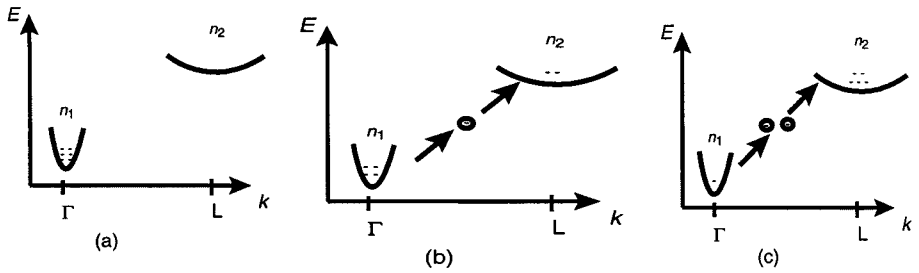

Fig. 10. Simplified energy-band diagram for a direct two-valley semiconductor showing electron transfer for: (a) $E < E_{\rm th}$, (b) $E > E_{\rm th}$, and (c) $E \gg E_{\rm th}$.

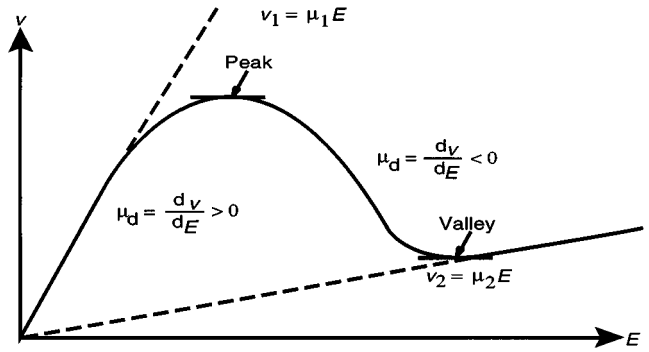

Fig. 11. v–E field profile for the two-valley semiconductor of Fig. 10.

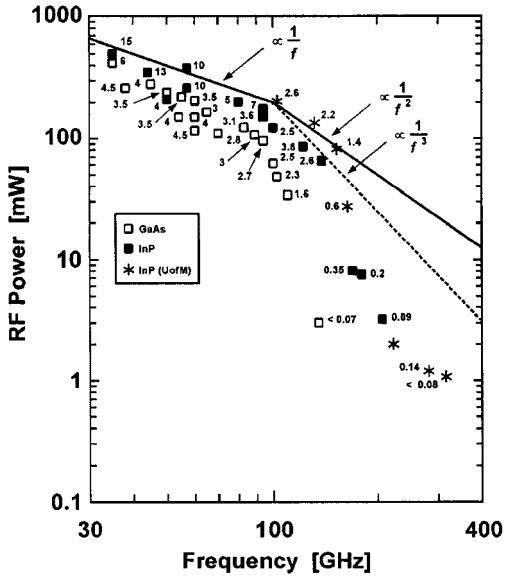

Fig. 12. Published state-of-the-art results from GaAs and InP Gunn devices under CW operation in the frequency range of 30–400 GHz. Numbers next to the symbols denote dc-to-RF conversion efficiencies in percent.

qualities.

1) It must have at least two valleys in the conduction band.
2) The minimum of the upper valley must be at least several kilotesla above the minimum of the lowest or main valley in the conduction band.
3) The energy difference between the minimum of the upper valley and that of the lower valley must be less than the energy gap Eg in order to avoid avalanche breakdown.
4) The transfer of electrons between the bands must take place in a time that is much less than the period of the operating frequency.
5) The effective mass of electrons in the upper valley must be much higher than that in the main valley and, thus, mobility in the upper valley will be much lower than in the main lower valley.

Fig. 10 shows a simplified band structure of such a material system, and Fig. 11 shows the v–E field characteristic, indicating the region of negative differential mobility $\mu_d < 0$, which is responsible for the negative resistance and, thus, power generation. It can be seen from these figures that when the electric field E is less than the so-called threshold field $E_{\rm th}$, most of the electrons will reside in the lower valley and have a high mobility. When $E > E_{\rm th}$, electrons in the main valley gain enough energy to transfer to the upper valley where the mobility is lower and, thus, the velocity decreases. This continues until the great majority of electrons are transferred to the upper valley and $E \gg E_{\rm th}$. The velocity then starts increasing again, but with a lower mobility.

Current oscillations in GaAs and InP were first observed by Gunn [14], [32] and were subsequently explained by the transferred-electron effect [16], [33]. Due to the negative differential mobility and depending on the doping concentration and length of the device, several modes of operation exist [34] and result in different properties of the device. The operating frequency is approximately given by

$$f_{op} = \frac{v_T}{l} \tag{23}$$

where $v_T =$ the effective transit velocity and $l =$ the length of the device. However, the operating frequency will vary from that given by (23) depending on the mode of operation. The bulk negative differential mobility alone does not result in a NDR at low frequencies, as seen previously in RTDs, but does result in a dynamic negative resistance at frequencies around f_{op}, as shown in [24]. Among the many semiconductor materials that exhibit the transferred-electron property, only two materials, namely, GaAs and InP, have received the most attention and resulted in the best performance. Since the relaxation rates in InP are smaller, InP has shown excellent performance up to very high frequencies [35]. Fig. 12 shows the state-of-the-art of GaAs and InP devices in the 30–300-GHz range.

C. Transit-Time Devices

This group includes several very important devices whose operation depends on a particular current injection mechanism and transit time to create the proper phase relationship between the RF voltage and current, which results in power generation. These devices have many common properties and their basic

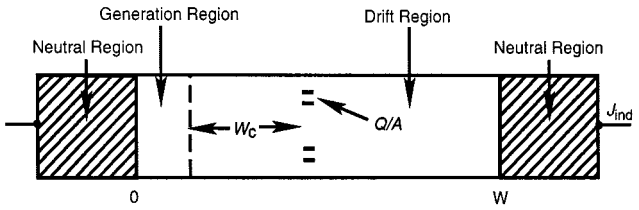

Fig. 13. Schematic longitudinal section of a negative-resistance transit-time diode.

principle of operation can be explained by reference to Fig. 13. In such devices, carriers are injected into a depleted region whose width is W and they drift toward the collector with a velocity that is dependent on the electric field in this region. Several mechanisms can be employed to generate and inject carriers. These include the following.

1) *Thermionic emission over a barrier*: Such a barrier can be formed by a p–n or Schottky junction in forward bias or by a heterojunction of a layer with a wider bandgap than in the neutral and drift regions. This would result in a BARITT device [22], [23].
2) *Tunneling through a barrier*: Electron tunneling takes place in a reverse-biased heavily doped p^+–n^+ junction. It can also take place through a heterojunction barrier and resonant tunneling through a double barrier. This would result in a TUNNET [21] or a quantum-well injection transit-time (QWITT) device [36].
3) *Avalanche multiplication through impact ionization*: At high electric fields in a reverse-biased p–n junction, electrons and holes gain enough energy to create additional carriers through ionization from the valence to the conduction band. This would result in carrier injection by avalanche breakdown and an IMPATT device [10].
4) At very high frequencies where very narrow regions of carrier generation exist, both tunneling and avalanche mechanisms are present and, thus, a mixed mode results. This would yield a mixed tunneling-avalanche transit-time (MITATT) device [37], [38].

The pulse of charge Q, which is injected into the drift region at location W_c, drifts under a high electric field at a drift velocity v_Q, and induces a current in the external circuit connected to the device. The induced current density in the external circuit is given by the Ramo–Shockley theorem [19]

$$J_{\text{ind}} = \frac{Q}{W}\left(v_Q - \frac{W_c}{W}\right)\frac{dW}{dt}. \tag{24}$$

Under ideal conditions, the diode is always punched through and the electric field is usually high enough so that the carrier velocity is saturated. Under these conditions, $v_Q = v_s$ and $dW/dt = 0$. Equation (24) reduces to

$$J_{\text{ind}} = \frac{Q}{W}\,v_s. \tag{25}$$

These properties allow us to use a simple and approximate large-signal analysis to determine the basic power generation capabilities of these devices. Under such large-signal conditions, we assume a sharp pulse of carriers is injected into the drift region and travels at a saturated velocity. This results in the voltage and current waveforms shown in Fig. 14 for all the transit-time devices described above.

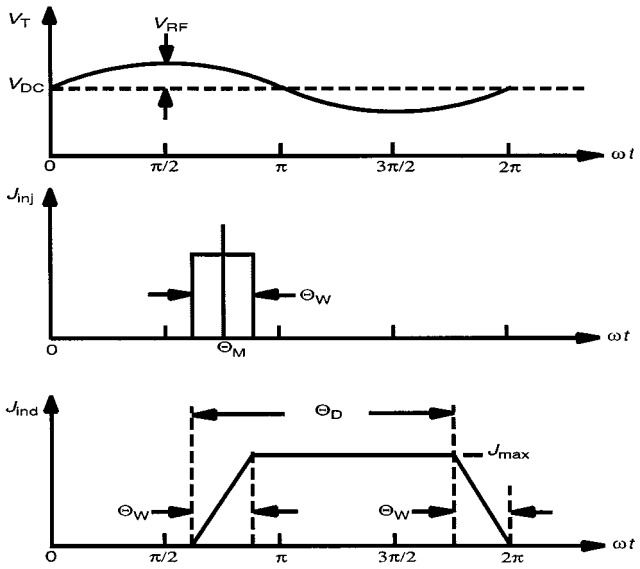

Fig. 14. Idealized voltage and current waveforms for transit-time diodes.

The voltage V_T across the diode is given by

$$V_T = V_{\text{DC}} + V_{\text{RF}} \sin \omega t \tag{26}$$

where V_{DC} and V_{RF} are the dc voltage and magnitude of the RF voltage, respectively. The current pulse is injected at phase angle θ_m with a width θ_w. The induced current is represented by the current density $J_{\max}$ and the transit angle in the drift region $\theta_D (= \omega W/v_s)$.

The properties of each of the devices under consideration are determined by θ_m, the injection phase angle, and θ_w, the effective width of the pulse. The RF power generated in such devices with area A is given by

$$P_{\text{RF}} = -\frac{A}{2\pi}\int_0^{2\pi} J_{\text{ind}}(\omega t) V_{\text{RF}} \sin \omega t \, d(\omega t) \tag{27}$$

which simplifies to

$$P_{\text{RF}} = A V_{\text{RF}} J_{\text{DC}} \frac{\sin(\theta_w/2)}{(\theta_w/2)} \frac{\cos(\theta_m + \theta_D) - \cos\theta_m}{\theta_D}. \tag{28}$$

The dc current density J_{DC} is given by

$$J_{\text{DC}} = \frac{1}{2\pi}\int_0^{2\pi} J_{\text{ind}}(\omega t)\, d(\omega t) = \frac{J_{\max}}{2\pi}\,\theta_D. \tag{29}$$

Therefore, the dc to RF conversion efficiency η is

$$\eta = \frac{P_{\text{RF}}}{P_{\text{DC}}} = \frac{V_{\text{RF}}}{V_{\text{DC}}} \frac{\sin(\theta_w/2)}{(\theta_w/2)} \frac{\cos(\theta_m + \theta_D) - \cos\theta_m}{\theta_D}. \tag{30}$$

It is clear from the above equations that it is desirable to have θ_w as small as possible. Under the ideal sharp pulse approximation, we assume $\theta_w = 0$. With this assumption, we can now determine the properties of the various transit-time devices as follows.

1) IMPATT Mode: In this mode, $\theta_m \cong \pi$ and (30) reduces to

$$\eta = \frac{V_{\rm RF}}{V_{\rm DC}} \left(\frac{\cos\theta_D - 1}{\theta_D} \right). \tag{31}$$

For $\theta_D = \pi$

$$\eta = \frac{-2}{\pi} \left(\frac{V_{\rm RF}}{V_{\rm DC}} \right)$$

and the maximum occurs at $\theta_D \approx 0.74\pi$ where

$$\eta = -\frac{2.27}{\pi} \left(\frac{V_{\rm RF}}{V_{\rm DC}} \right).$$

IMPATTS are very efficient relative to the other devices and generate very high power. This is because $V_{\rm RF}/V_{\rm DC}$ can approach 60% in materials such as GaAs and InP and efficiencies can approach 40% under ideal conditions. Also, the current density in IMPATTS is very high and, thus, the power output will also be high. IMPATTS, therefore, are the most powerful solid-state devices available. However, they are quite noisy because of the avalanche generation mechanism. The noise can be reduced by injection locking or by introducing a tunneling component to the injection mechanism as will be discussed below.

2) TUNNETT and BARITT Modes: In these modes, $\theta_m = \pi/2$ and η becomes

$$\eta = \frac{V_{\rm RF}}{V_{\rm DC}} \frac{\sin\theta_D}{\theta_D}. \tag{32}$$

In this case, η is maximum at $\theta_D = 3\pi/2$, where $\eta = (-2/3\pi)(V_{\rm RF}/V_{\rm DC})$.

As can be seen from these expressions, the efficiency of TUNNETT and BARITT devices is approximately 1/3 that of an IMPATT under ideal conditions. This is because there is an induced current during the positive half of the RF cycle extending from $\theta = \pi/2$ to π and, thus, the device absorbs power during this phase. However, $V_{\rm DC}$ will be higher and the capacitance lower, which will have a positive effect on power output. In addition, because of the carrier generation process, these devices have excellent noise performance, which is comparable to TEDs [24].

3) MITATT Mode: In this mode of operation, θ_m varies from $\pi/2$ to π depending on the ratio of tunneling to avalanche generation and, therefore, the efficiency and power output will vary between a pure TUNNETT and a pure IMPATT mode.

4) QWITT Mode: In this mode of operation, $\theta_m \cong 3\pi/2$ and η becomes

$$\eta = -\frac{V_{\rm RF}}{V_{\rm DC}} \frac{\sin\theta_D}{\theta_D}. \tag{33}$$

For $\theta_D = \pi/2$

$$\eta = \frac{-2}{\pi} \frac{V_{\rm RF}}{V_{\rm DC}}.$$

As can be seen, the efficiency expression becomes the same as for an IMPATT, however, in this case, $V_{\rm DC}$ and $V_{\rm RF}$ will be very small and power generation will be small. Also, as discussed earlier, such a device is more difficult to stabilize because the negative resistance will extend to dc, which will limit the power further.

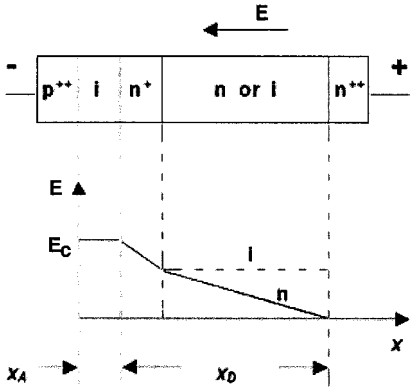

Fig. 15. Schematic layer sequence and electric-field profile for single-drift transit-time diodes.

D. Device Structures for Transit-Time Devices

The basic device structure for IMPATT, MITATT, and TUNNETT devices is shown in Fig. 15, where E_c is the critical field for breakdown. The generation region width x_A can be controlled by the width of the i layer at the p^+in^+ junction, and this will result in the following different modes of operation:

For $x_A > 100$ nm, $E_c x_A = 1$, we get avalanche breakdown and, thus, an IMPATT diode. For $x_A < 50$ nm, $E_c > 10^6$ V/cm, we get mostly tunneling and, thus, a TUNNETT diode. For 50 nm $< x_A <$ 100 nm, we have mixed tunneling and avalanche breakdown, and this results in an MITATT diode.

As the frequency of operation gets higher, the depletion layer widths become smaller and it becomes more difficult to control the width of x_A. At extremely high frequencies, it becomes difficult to satisfy the relationship of $E_c x_A = 1$ and, thus, would be difficult to operate in the IMPATT mode (unless we use very high E_c materials) and, in this case, the TUNNETT mode will dominate. It is, therefore, expected that TUNNETT devices will be more suitable for frequencies approach the terahertz region.

From the approximate waveforms shown earlier, it is relatively straightforward to estimate the power and efficiency of these devices after a structure as shown in Fig. 15 is chosen. This is beyond the realm of this review and the reader is referred to [24], [38]–[41].

IMPATT devices in particular can also be implemented in so called double-drift structures, as shown in Fig. 16. Here, the generation region is in the middle and both electron and hole drift regions are present, but the basic operation is the same. Here, the electronic power generation capability is approximately four times as large as that of single drift devices. The reason for this is the lower capacitance, which is one-half and, thus, the area can be made twice as large for the same impedance level. The breakdown voltage will be double and, thus, for the same current density, we get twice the voltage and twice the current and, thus, the power will be four times higher. However, the thermal resistance will be higher and, therefore, the CW operation we get is approximately twice the power, which is still substantial.

The basic device structure and electric-field profile for a BARITT device at the operating point are shown in Fig. 17. It is shown that there is a small region at the forward-bias injection point where the electric field is below the $v_{\rm sat}$ region for carriers, but the carriers become saturated when $E > E_s$.

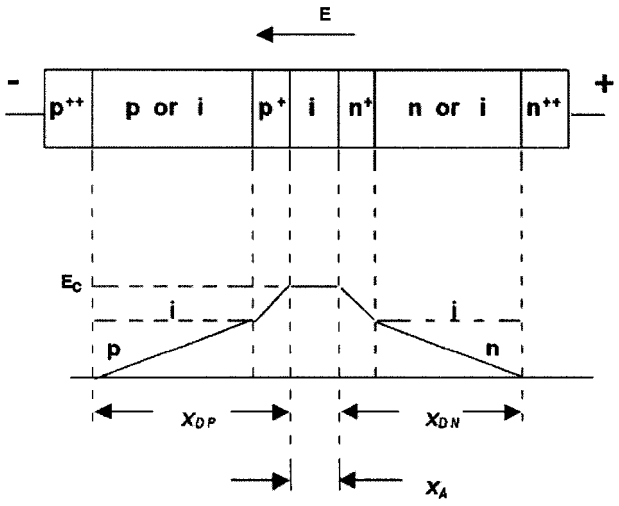

Fig. 16. Schematic layer sequence and electric-field profile for double-drift transit-time diodes.

Due to the basic mechanisms involved in the forward-bias junction region, the ratio of $V_{\rm RF}/V_{\rm DC}$ is limited to small values and, thus, the achieved efficiency is much smaller than the ideal value cited previously. Again, here, we can estimate the power output and efficiency after the structure is chosen, and the reader is referred to several references on this subject [42]–[44].

The state-of-the-art CW experimental results of these transmit time devices are shown in Fig. 18. Of course, significantly more power can be generated under pulse conditions where thermal considerations are relaxed. Transit-time devices so far have been realized mostly in Si and GaAs. Other materials such as InP and more recent ones such as SiC [45] and GaN, which have a larger E_c, may be capable of generating significantly higher powers. It is well known that the basic material parameters that determine the power generation capability are the critical field for breakdown E_c and the saturated velocity. In addition, the conversion efficiency from dc to RF is also important, and this depends on the mode of operation and other basic material properties such as low field mobility and ohmic contacts. Therefore,

$$P_{\rm RF}({\rm Gen.})\alpha(E_c v_s)^2\eta. \tag{34}$$

The figure-of-merit $(E_c v_s)^2$ is given in Table I for several material systems and it is seen from this table that some materials have a much greater potential that has yet to be tapped. Ultimately, of course, the large E_c and velocity occur in vacuum and, thus, tunnel transit-time devices based on tunneling from cold cathodes in vacuum where electrons travel ballistically in the drift region may be very appropriate for terahertz power generation as has already been proposed [46].

V. Three-Terminal Devices

The earliest development work with microwave solid-state devices were attempts to fabricate three-terminal devices in semiconductors. Transistor structures have always been favored by circuit designers due to the inherent isolation between the input and output ports, and the resulting simplification in circuit design. This permits oscillators and amplifiers to be fabricated without the use of nonreciprocal devices such as circulators, which tend to be large and temperature sensitive due to the use of magnetic materials. Transistor structures, however, are generally more difficult to fabricate than two-terminal devices, and advanced high-performance transistors required the development of advanced lithography and fabrication technology that permitted submicrometer feature size to be realized. Minimum feature size on the order of 0.1 μm and below is now readily available using electron-beam lithography and high-performance microwave and millimeter-wave transistors can be fabricated and are finding commercial application.

Both bipolar and field-effect transistors are used for microwave and millimeter-wave application. Standard Si bipolar transistors can be used to about Ka-band (26–40 GHz), and HBTs using the AlGaAs/GaAs or InGaAs/InP material systems extend the upper frequency of operation to over 100 GHz. Field-effect transistors, primarily due to the ability to realize submicrometer gatelengths, are near ideal for high-frequency operation and are routinely used for microwave applications up to 100 GHz. Use of heterostructures to realize HEMTs or HFETs extend the upper frequency of operation to around 300 GHz. The basic operation and performance of bipolar and field-effect transistors are presented in this section.

A. Bipolar Transistors

The bipolar transistor was invented by Shockly, Bardeen, and Brittain in 1948 [2], [3]. Since that time, the device has undergone continued development and improvement and is now in wide use for microwave and millimeter-wave applications. The majority of bipolar transistors are fabricated from Si and are useful for microwave applications through about C-band and up to X-band. Although the advantages of utilizing a wide-bandgap semiconductor for the emitter of a bipolar transistor were discussed by Shockley in his transistor patent, the modern HBT was proposed in 1957 by Kroemer [47], who also discussed the advantages of HBTs over conventional bipolar transistors. Significant development followed and promising results started to appear in the 1970s [48]–[53] with HBT development in III–V compound semiconductors based upon the AlGaAs/GaAs system. However, it was not until the development of MBE semiconductor growth technology that practical heterojunctions of sufficient quality for practical device application could be produced and, by the 1980s, the technology of fabricating HBTs with excellent microwave performance was advancing [48]–[53]. By the early 1990s, the current gain frequency response of these devices had reached 200 GHz [53]. Submicrometer scaling has now pushed the f_Ts to the range of 300 GHz [54]. The development of HBTs using SiGe as the base were reported in 1987 [55], and these devices advanced rapidly and now produce RF performance essentially equivalent to AlGaAs/GaAs HBTs. The SiGe material is used as the base region, and since SiGe has a smaller bandgap than Si, a device with the advantages of a wide bandgap emitter are obtained. The SiGe–Si HBT has the advantage of being compatible with standard Si processing technology, which makes the device attractive from a cost perspective.

1) Basic Operation Principles: The bipolar transistor is a p-n junction device and is formed from back-to-back junctions.

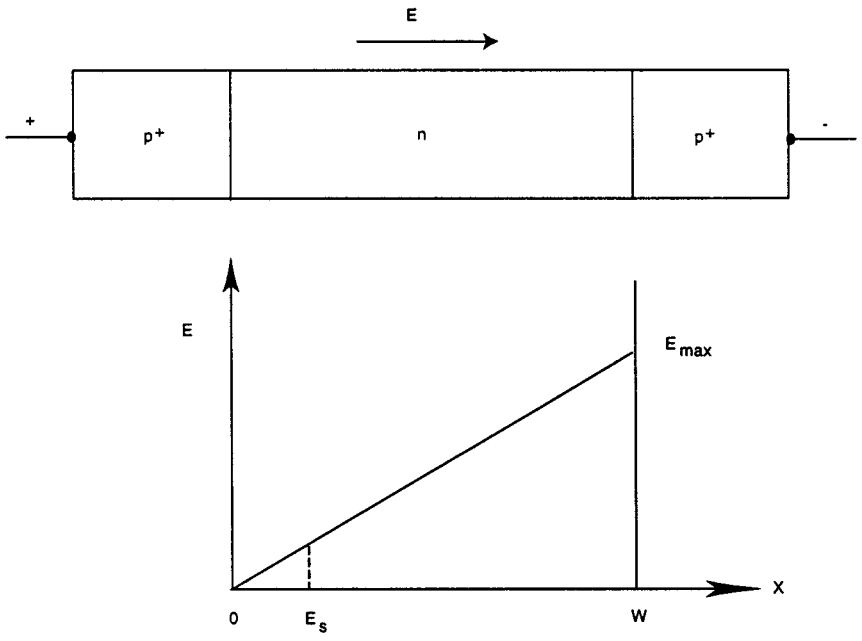

Fig. 17. Basic device structure and electric-field profile for a BARITT diode.

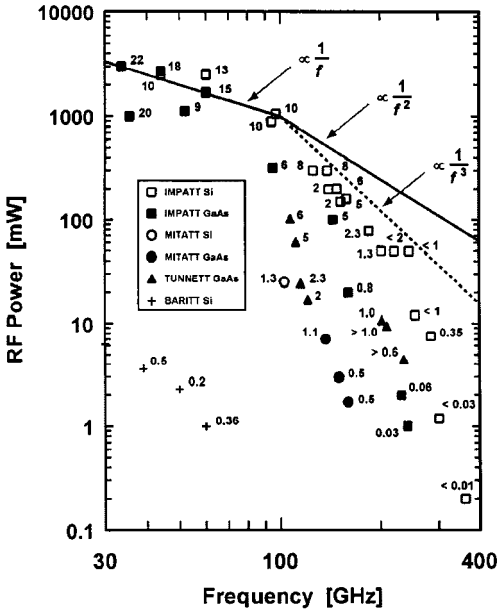

Fig. 18. State-of-the-art RF power levels from transit-time diodes under CW operation in the frequency range of 30–400 GHz. Numbers next to the symbols denote dc-to-RF conversion efficiencies (in percents).

Since it is a three-terminal device, it can be either p-n-p or n-p-n. For high-frequency application, the n-p-n structure is preferred because the operation of the device is dependent upon the ability of minority carriers to diffuse across the base region. Since electrons have superior transport characteristics compared to holes, the n-p-n structure is indicated.

The microwave operation of a bipolar transistor is dependent upon the time for a charge carrier to transit the entire length of the device [56], [57]. The physical structure for the transistor is shown in Fig. 19 and the energy band diagram is shown in Fig. 20.

In normal operation, the base–emitter junction is forward biased and the base–collector junction is reverse biased. Electrons are injected from the emitter into the base region where they travel by diffusion transport to the collector junction. At the collector, they are attracted by the reverse-bias field and swept into the collector region. The transit time through the transistor can be written as the sum of five transit times, and expressed as

$$\tau_{ec} = \tau_e + \tau_e' + \tau_b + \tau_c + \tau_c' \tag{35}$$

where τ_{ec} is the total emitter-to-collector transit-time, τ_e is the base–emitter capacitance charging time, τ_e' is the base–emitter depletion region transit-time, τ_b is the base region transit time, τ_c is the base–collector capacitance charging time, and τ_c' is the base–collector depletion region transit time. For a standard Si bipolar transistor, the base–emitter region transit time is generally small and can be neglected since the junction is forward biased. The gain-bandwidth product f_T for the transistor is the reciprocal of the total transit time, and can be expressed as [56], [57]

$$f_T = \frac{1}{2\pi\tau_{ec}} \cong \left\{2\pi\left[\frac{kT(C_e + C_c + C_p)}{qI_C} + \frac{W_B^2}{\eta D_{pB}} + \frac{x_c - W_B}{2v_s}\right]\right\}^{-1}. \tag{36}$$

Typically, for a microwave bipolar transistor designed to operate at frequencies up to about S-band, the emitter-to-collector transit time divides in the following manner:

$$\tau_e \sim 40\%\,\tau_{ec} \quad \tau_b \sim 10\%\,\tau_{ec} \quad \tau_c' \sim 45\%\,\tau_{ec} \quad \tau_c \sim 5\%\,\tau_{ec}$$

and the frequency response of the transistor is primarily limited by the base–emitter capacitance charging time, and the base–collector depletion region transit time. However, for

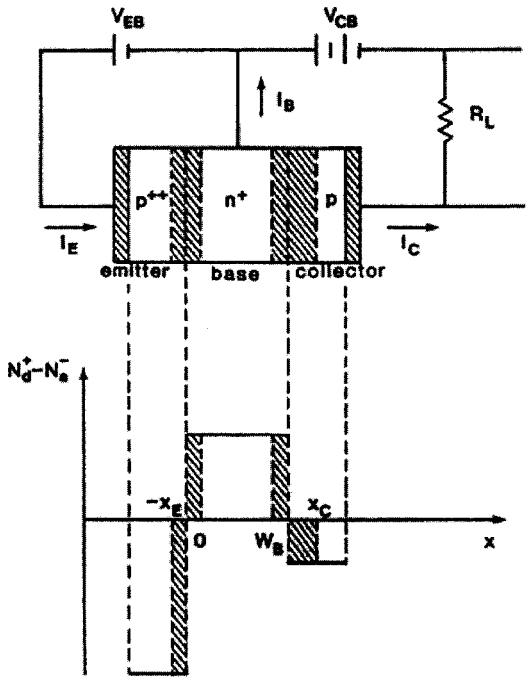

Fig. 19. Basic structure for a bipolar transistor.

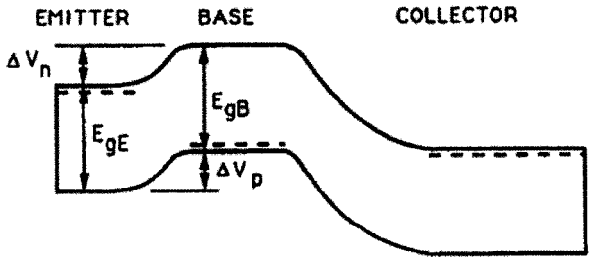

Fig. 20. Energy band diagram for a bipolar transistor.

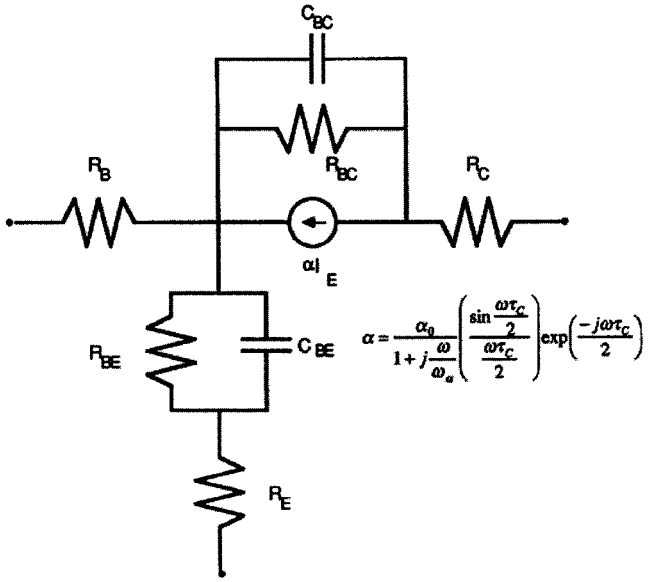

Fig. 21. Bipolar transistor equivalent circuit.

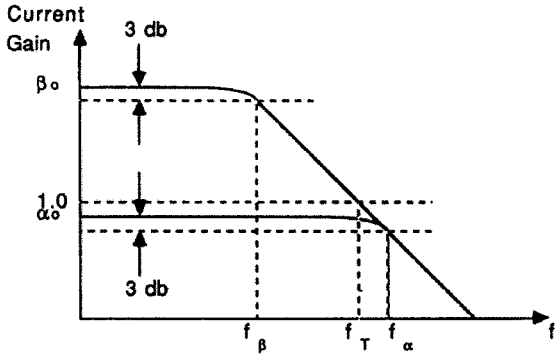

Fig. 22. Current gain versus frequency for a bipolar transistor.

transistors optimized for higher frequencies, the capacitance charging times are minimized by area reduction and doping profile optimization and the transit times across the base region and the base–collector depletion regions will dominate the frequency response. Si bipolar transistors can be designed to operate with good gain performance up to Ka-band.

To improve the frequency response and RF performance of the bipolar transistor, a wide-bandgap semiconductor can be used as the emitter. In order to achieve good performance, it is desirable for the emitter current injected into the base to consist essentially entirely of minority current in the base region. The currents in the base and emitter regions, however, consist of both minority and majority currents, and some majority current in the base is back injected into the emitter, where it degrades transistor performance. The back-injected current degrades the current injection efficiency and reduces transistor gain. In a standard bipolar transistor, the back injection can only be minimized by fabricating the device with an emitter impurity concentration much larger than that in the base, typically by one to two orders of magnitude. However, by introduction of a wide-bandgap semiconductor for the emitter, the back injection of current can be blocked by the energy band discontinuity. The emitter region doping can, therefore, be optimized for transistor performance without back injection concerns. This is the advantage of the HBT noted by Shockly in his original transistor patent. The heterojunction bandgap can be chosen so that the HBT will have current gain independent of the base and emitter doping. This permits fabrication of a microwave transistor with a heavily doped base region and a lightly doped emitter region. Therefore, compared to a standard bipolar transistor, the HBT has reduced base resistance, output conductance, and emitter depletion capacitance, and greatly improved high-frequency performance.

A high-frequency equivalent circuit for the bipolar transistor is shown in Fig. 21. The basic Ebers–Moll or Gummel–Poon models can be used, suitably modified to account for parasitic effects, etc. Charge control model formulations have proved successful and many variations have been presented.

The current gain for the transistor as a function of frequency is shown in Fig. 22. The current gain at microwave frequencies decreases inversely proportional to frequency, as indicated, and in the common-emitter configuration f_T indicates the upper frequency at which positive current gain β exists. In the common-base configuration, the current gain α is always less than unity.

Examination of the equivalent circuit yields an expression for unilateral gain of the transistor

$$U \cong \frac{\alpha_o}{16\pi^2 r_b C_c f^2 \left(\tau_{ec} + \dfrac{r_{be} C_{bc}}{\alpha_o}\right)} \tag{37}$$

where α_o is the common-base dc current gain indicated in Fig. 22. The unilateral power gain represents the maximum gain possible from the transistor when it is embedded in a network with no feedback paths. The unilateral gain is an inverse function of the square of the frequency, and U, therefore, decreases at a -6 dB/octave rate. The frequency at which the gain is reduced to unity is called the maximum frequency of oscillation ($f_{\max}$), and is a useful figure-of-merit for the transistor. It represents the greatest frequency at which the transistor has active power gain and, in terms of the equivalent-circuit parameters, can be expressed as

$$f_{\max} = \left[\frac{f_T}{8\pi r_b C_c}\right]^{1/2}. \tag{38}$$

The ability to employ highly doped base regions permits low base region resistance r_b to be obtained. Primarily for this reason, HBTs have excellent high-frequency performance capability. They produce increased f_T compared to standard bipolar transistors and $f_{\max}$ approaching 200 GHz has been obtained.

A comparison of gain-bandwidth products for similar GaAs and SiGe HBTs has been reported by Ning [58]. A GaAs HBT with a 0.6 $\times$ 4.6 μm^2 emitter produced an f_T of 140 GHz, whereas an SiGe HBT with a 0.35 $\times$ 3.55 μm^2 emitter produced an f_T of 130 GHz. The peak f_T occurs at slightly lower collector current for the GaAs HBT compared to the SiGe HBT. These results indicated that the two HBTs have comparable high-frequency performance. The SiGe–Si HBTs also have excellent low-noise performance due to high mobility in the SiGe material, which helps produce a low base resistance.

2) Noise Figure: Noise figure is a measure of the amount of noise added to a signal by a lossy device through which the signal passes. It is defined as the ratio of the input to output signal-to-noise ratios and is generally expressed in decibels according to the expression

$$F = 10 \log \frac{(\mathrm{S/N})_{\mathrm{in}}}{(\mathrm{S/N})_{\mathrm{out}}}. \tag{39}$$

In terms of the equivalent-circuit parameters, the minimum noise figure for the transistor can be expressed as

$$F_{\min} = a \frac{r_b + R_{\mathrm{opt}}}{r_e} + \left(1 + \frac{f^2}{f_b^2}\right) \frac{1}{\alpha_o} \tag{40}$$

where the optimum source resistance is

$$R_{\mathrm{opt}} = \left\{ r_b^2 - X_{\mathrm{opt}}^2 + \left(1 + \frac{f^2}{f_b^2}\right) \frac{r_e(2r_b + r_e)}{\alpha_o a} \right\}^{1/2} \tag{41a}$$

and the optimum source reactance is

$$X_{\mathrm{opt}} = \left(1 + \frac{f^2}{f_b^2}\right) \frac{2\pi f C_{TE} r_e^2}{\alpha_o a} \tag{41b}$$

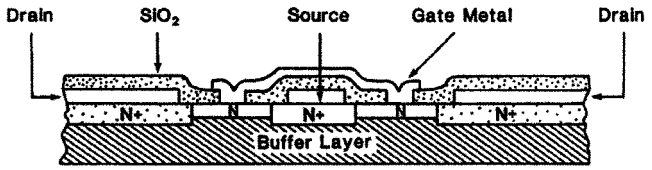

Fig. 23. Basic structure for a field-effect transistor.

where

$$a = \left\{ \left(1 + \frac{f^2}{f_b^2}\right)\left(1 + \frac{f^2}{f_e^2}\right) - \alpha_o \right\} \frac{1}{\alpha_o}. \tag{41c}$$

The f_b and f_e terms represent the base and emitter–base junction cutoff frequencies.

Typically, Si bipolar transistors have a noise figure less than 1 dB up to about 2–3 GHz, and noise figures in the range of 3 dB up through X-band. HBTs have improved performance and noise figures in the range of 2 dB at K-band can be obtained. SiGe HBTs produce noise figures just under 2 dB at X-band and in the range of 3 dB at 20 GHz.

B. Field-Effect Transistors

The modern field-effect transistor derives from the early work of Stuetzer in 1950 [6] and Shockley in 1952 [8]. The basic structure, which was based upon the vacuum triode, is shown in Fig. 23, and consists of two conducting electrodes (the source and drain) located on the surface of a conducting semiconductor layer. The FET structure shown in Fig. 23 has two drain contacts and two gates, and is typical of practical devices.

The electrode contacts are designed to have ohmic characteristics (facilitated by the N^+ regions) so that when connected to an external bias source, the device operates as a simple resistor. A third electrode (the gate) is located between the two electrodes and is designed to be a rectifying contact. By applying a reverse bias, the channel region under the gate can be depleted of charge, thereby providing a gating function. Since application of a small RF signal to the gate permits control of the channel current, which is relatively large, a gain mechanism is established. The rectifying gate contact can either be a metal–semiconductor Schottky contact to form a MESFET, or a p-n junction to form a junction field-effect transistor (JFET). In general, RF performance of the MESFET has proven much superior to that of the JFET and development work with JFETs has been limited.

The early FET development work was hindered by poor semiconductor quality, large feature size that could be produced with available patterning techniques, and difficulty in obtaining suitable low-resistance contacts. The large gatelengths that could be produced resulted in very low gain and very low frequency response. Most development work shifted to the bipolar transistor since the performance of this device was less sensitive to geometry limitations. Serious development work with the field-effect transistor reemerged in the late 1960s with the development of projection photomasking technology that permitted the small feature size required for high-performance transistors to be realized. For example, in 1969, Middelhoek [59] demonstrated a silicon MESFET with a 1-μm gatelength. Using this technology, a transistor with X-band performance

(i.e., $f_{\max} = 12$ GHz) was produced [60], which was equivalent to the best $f_{\max}$ available from bipolar transistors at the time. Although other work was pursued using silicon, including some work with JFETs, most attention soon shifted to the use of GaAs due to the higher mobility available with this semiconductor. This work was successful and high-performance MESFETs were soon realized. For example, fabrication of a 1-μm gatelength GaAs MESFET with an $f_{\max}$ of 50 GHz, and useful gain up to 18 GHz [61] was reported in 1970. As the importance of gatelength control and the relationship of gatelength to microwave performance was understood, there was effort directed toward development of advanced lithography technology that could produce less than 1-μm minimum feature size. Electron-beam lithography was rapidly developing and was applied to define gates [62] for GaAs MESFET fabrication. This technology has improved steadily and can now routinely produce gatelengths down to 0.1 μm and less. At the present, time high-performance FETs for most microwave and virtually all millimeter-wave applications have gates defined by electron-beam lithography.

The GaAs MESFET developed rapidly and, by 1972, it was clear that these devices were capable of very low-noise amplification [63], and noise figures in the range of 3–4 dB were obtained at X-band. Improved material and contact technology and gatelength reduction have permitted noise figures to be continually reduced and noise figures on the order of 1–2 dB in X-band and 3–4 dB in Ka-band can now be obtained. The GaAs MESFET can be redesigned for microwave power applications by using multiple gate fingers arranged in parallel. This permits large gatewidths to be fabricated while maintaining the short gate necessary for microwave performance. Since channel current is directly proportional to gatewidth, the multiple gate finer structure results in large RF power due to the increased RF currents that flow. The first devices using this technique were demonstrated in 1973 [64]–[66]. A GaAs MESFET with 20 gates, each 1-μm long and 400-μm wide, permitted S-band power of 1.6 W with 5-dB gain and 21% power-added efficiency to be obtained [64]. Power devices have rapidly developed and today MESFETs with S-band power greater than 80 W- and Ka-band power approaching 1 W are commercially available.

HEMTs: Field-effect transistors based upon heterojunctions can also be fabricated. These devices make use of the modulation doping principle proposed by Esaki and Tsu in 1969 [67], as shown in Fig. 24.

Free charge from the high doped regions diffuses into the low doped regions where it is able to flow with high mobility due to the lack of impurity scattering in the low doped regions. High current results. If the high doped region is fabricated from a semiconductor with a wider bandgap, than the low doped regions and the discontinuity in the energy bands is restricted to the conduction band, a quantum well is created in the conduction bands at the interface between the two semiconductors. As electrons from the wide-bandgap semiconductor diffuse into the quantum well, a two-dimensional electron gas (2DEG) is created, as shown in Fig. 25.

The concept was demonstrated by Stormer in 1979 [68]. The 2DEG can be used to form the channel region for a field-effect transistor, as shown in Fig. 26.

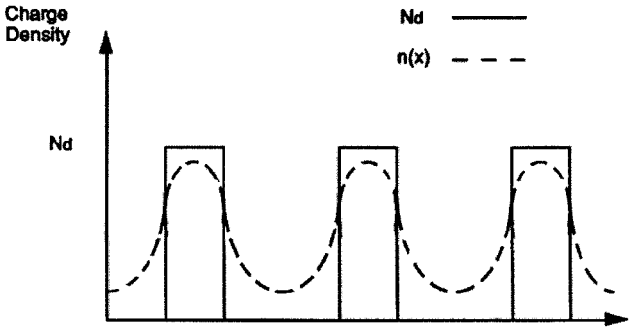

Fig. 24. Modulation doping principle.

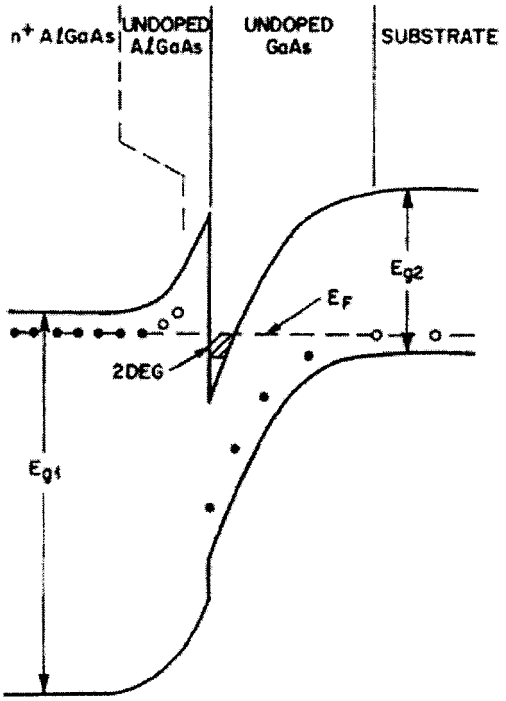

Fig. 25. Formation of a 2DEG at a heterointerface between wide- and narrow-bandgap semiconductors.

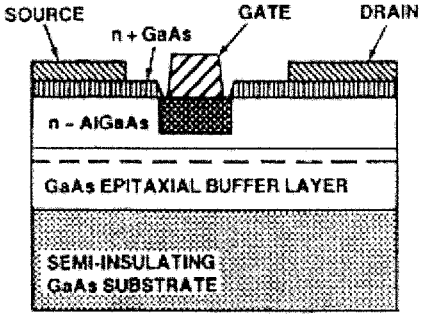

Fig. 26. HEMT structure.

The resulting transistor is called a HEMT and was demonstrated by Mimura in 1980 [69]. HEMTs have extremely high-frequency performance capability and very low-noise performance, primarily due to the very high mobility characteristics of the 2DEG. These devices are also used for microwave and

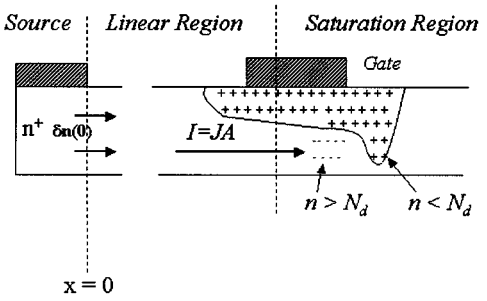

Fig. 27. MESFET conducting channel.

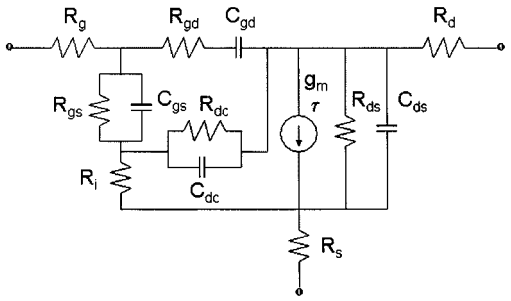

Fig. 28. Field-effect transistor equivalent circuit.

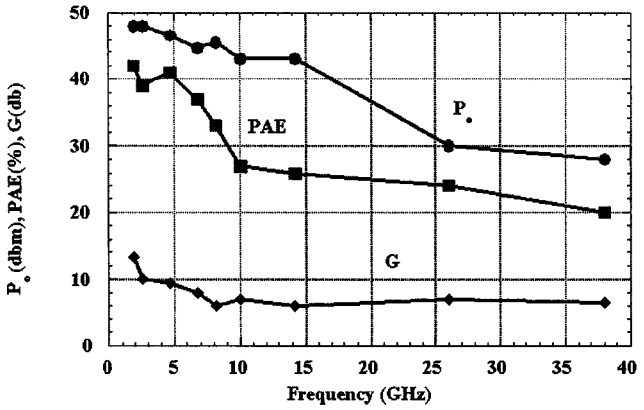

Fig. 29. RF performance of commercially available power FETs.

millimeter-wave power applications and above X-band are superior to MESFETs. The HEMT is described in more detail by Mimura elsewhere in this TRANSACTIONS.

Basic Operation Principles: The basic operation of a field-effect transistor is illustrated in Fig. 27. In normal operation, the drain is biased with a positive voltage and the source is grounded. Electrons are, therefore, injected from the source into the conducting channel where they form the channel current. The gate is reverse biased, forming a depletion region under the gate.

As the voltage applied to the gate is modulated by an RF signal, the depletion region will vary in the conducting channel with a depth proportional to the magnitude of the applied gate voltage. When the depletion region extends through the entire conducting channel, a pinchoff condition is achieved. For gate bias voltages that vary between open channel and pinchoff conditions, a set of well-known saturating I–V characteristics result. Key parameters can be derived from a simple model and are the pinchoff voltage

$$V_{po} = \left(\frac{qN_d}{2\varepsilon}\right) a^2 \tag{42}$$

the transconductance

$$g_m = \frac{I_s}{2V_{po}} \left[\frac{1}{1 - I_d/I_s}\right] \tag{43}$$

and gate–source capacitance

$$C_{gs} \cong 2\varepsilon Z \left[\frac{L}{a}\left(\frac{1}{1 - I_d/I_s}\right) + 1.56\right] \tag{44}$$

where N_d is the channel doping density, a is the conducting channel thickness, L is the gatelength, Z is the gatewidth, I_d is the drain current, and I_s is the maximum saturation current. An equivalent circuit for the field-effect transistor is shown in Fig. 28.

An analysis of the equivalent circuit for the FET yields an expression for the current gain-bandwidth product that can be written as

$$f_T = \frac{g_m}{2\pi C_{gs}} \cong \frac{v_s}{2\pi L} \tag{45}$$

where v_s is the saturation velocity of the electrons in the conducting channel. High current gain and high frequency response require short gatelengths and high electron saturation velocity. The former is controlled by the lithography and process technology employed to fabricate the gate and the latter is a function of the semiconductor. Similarly, the maximum frequency of oscillation can be derived from the equivalent circuit and is

$$f_{\max} = \frac{f_T}{2}\sqrt{\frac{R_{ds}}{R_g}}. \tag{46}$$

A high $f_{\max}$ requires a high f_T and a large R_{ds}/R_g ratio. The f_T represents current gain and the R_{ds}/R_g ratio represents voltage gain. Power gain can be obtained at frequencies above f_T, but only by establishing suitable voltage gain and this requires large output impedance to input impedance ratios. This is difficult to achieve at microwave frequencies and high-performance millimeter-wave devices require high f_T.

RF Power Performance: By scaling gatelength to the range of $L_g = 0.1$ μm and by increasing channel doping to the range of $N_d \sim 10^{18}$ cm^{-3}, state-of-the-art GaAs MESFETs have f_Ts on the order of 100 GHz, and can operate with good RF power, gain, and efficiency at least through Ka-band. HEMTs can be optimized to operate with f_Ts greater than 300 GHz, and are generally used for most applications above X-band. FETs can be optimized for maximum RF output power by using gatelengths on the order of $L_g = 0.5$ μm and by reducing channel doping to increase gate-drain breakdown voltage. Power designs also require device and package designs that produce reduced thermal resistance. Power FETs that produce on the order of 80 W at S-band and almost 1 W at 40 GHz with good power-added efficiency and gain, as shown in Fig. 29, are now commercially available.

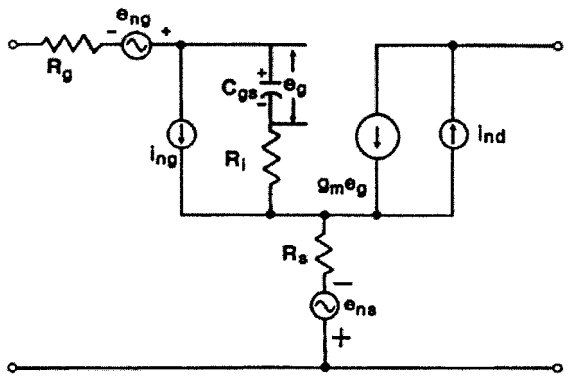

Fig. 30. FET equivalent circuit used for noise calculations.

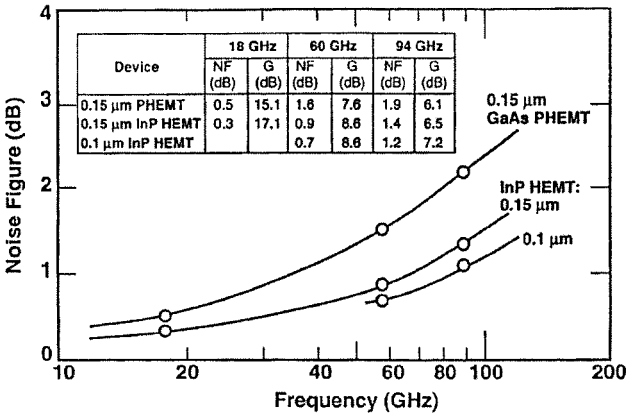

Fig. 31. Noise-figure performance for HEMTs.

Noise-Figure Performance: The noise figure of a MESFET or HEMT can be calculated from a simplified equivalent circuit, as shown in Fig. 30.

The minimum noise figure can be written as [70]

$$F_{\min} \cong 10 \log \left[1 + KfL\sqrt{g_m(R_g + R_s)} \right] \qquad (47)$$

where K is a fitting factor selected to match experimental data. This expression indicates the advantage in short gatelengths and low parasitic resistances for low-noise transistors. State-of-the-art FETs utilize gatelengths in the range of 0.1–0.2 μm and typically demonstrate minimum noise figures in the range of 1–2 dB through K-band. At lower frequencies, minimum noise figure in the range of 0.3–0.5 dB are typically obtained up to X-band. The noise performance of HEMTs optimized for low-noise performance as a function of frequency is shown in Fig. 31. As shown, HEMTs produce noise figures on the order of 0.2–0.3 dB at X-band and noise figure approaching slightly greater than 1 dB at 100 GHz. These devices produce excellent low-noise amplifiers for millimeter-wave applications.

Wide-Bandgap Semiconductor Transistors: Wide-bandgap semiconductors show great promise for advancing the state-of-the-art for high-power microwave electronic devices. Primarily due to low breakdown voltage of traditional semiconductors, it has not been possible to design and fabricate solid-state transistors that can yield RF output power on the order of hundreds to thousands of watts necessary to compete with microwave vacuum tubes for high-power applications. This has severely limited the use of microwave solid-state transistors and devices in high-power applications, such as transmitters for wireless communications systems, radars, HDTV, etc. Recent improvements in the growth of wide-bandgap semiconductor materials, such as SiC and the GaN-based alloys, provide the opportunity to now design and fabricate microwave transistors that demonstrate performance previously available only from microwave tubes. The most promising electronic devices for fabrication in wide-bandgap semiconductors for these applications are MESFETs fabricated from 4H-SiC and HFETs fabricated using the AlGaN/GaN heterojunction.

The advantages of device fabrication from wide-bandgap semiconductors can be seen from a comparison of fundamental electronic transport and material parameters, as shown in Table I. SiC and GaN have energy bandgaps about two to three times those in the conventional semiconductors such as Si, GaAs, and InP. The dielectric constant is about 20% lower than the conventional materials, and this permits a wide-bandgap semiconductor device to be about 20% larger in area for a given impedance and thereby allowing greater current. The thermal conductance of the material is extremely important and SiC is an excellent thermal conductor, while GaN is about the same as Si, the best of the conventional semiconductors. Finally, the critical electric field for electronic breakdown should be high. This parameter is an indication of the strength of the electric fields that can be supported internally to the device before breakdown. High electric fields permit large terminal RF voltages to be supported, and this is necessary for the generation of high RF power. The critical fields for the wide-bandgap materials are excellent and very high, typically an order of magnitude greater than for the conventional semiconductors. In general, the wide-bandgap semiconductors have more optimum values for all these parameters compared to conventional semiconductors.

A current is determined by the ease with which it can travel through a material. Generally, high mobility and saturation velocity are desirable and result in high current capability. Although SiC and GaN have relatively low values for the charge carrier mobilities (typically, $\mu_n \sim$ 200–500 cm^2/V $\cdot$ s), they have very high saturation velocity (typically, $v_s \sim 2{\times}10^7$ cm/s). The electron saturation velocity in both 6H- and 4H-SiC is $v_s \sim 2 \times 10^7$ cm/s, which is a factor of two higher than for Si ($v_s \sim 1 \times 10^7$ cm/s) and a factor of four higher than for GaAs ($v_s \sim (0.5\text{–}0.6) \times 10^7$ cm/s). Also, the mobility and saturation velocity for the 2DEG for the AlGaN/GaN heterointerface is very suitable for device applications. The room-temperature mobility of the 2DEG is in the range of 1000–1500 cm^2/V $\cdot$ s, which is significantly better than for SiC or bulk GaN. The sheet charge density for this structure can be very high and greater than $n_s \sim 10^{13}$ cm^{-2} due to piezoelectric and spontaneous polarization induced effects, and the measured sheet charge density is about a factor of five better than is obtained for the more commonly employed AlGaAs/GaAs heterostructure.

The predicted RF performance of 4H-SiC MESFETs and AlGaN/GaN HFETs as a function of frequency are shown in

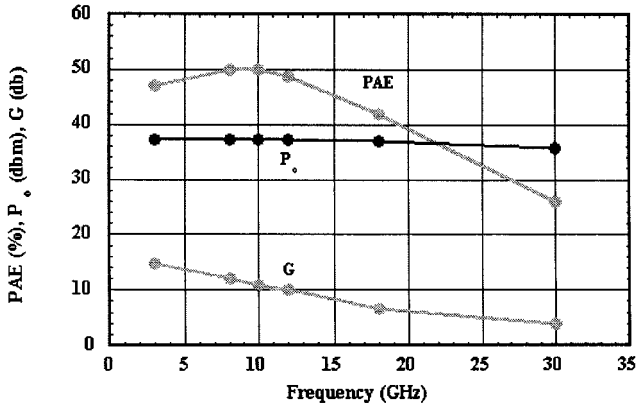

Fig. 32. RF performance for a 1-mm gatewidth 4H-SiC MESFET class-A amplifier.

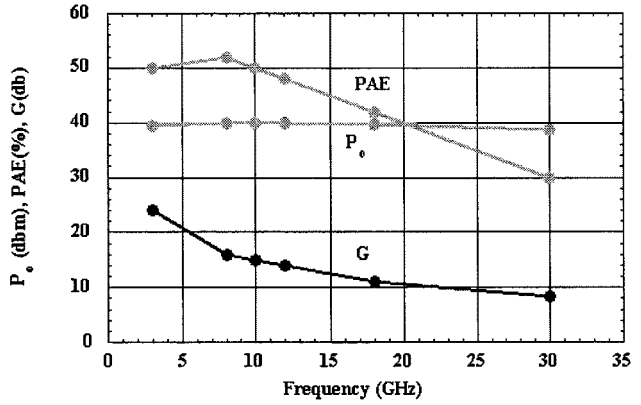

Fig. 33. RF performance for a 1-mm gatewidth AlGaN/GaN HFET class-A amplifier.

Figs. 32 and 33, respectively. 4H-SiC MESFETs can produce RF output power on the order of 4–6 W/mm, and should produce useful RF power through X-band [71]. AlGaN/GaN HFETs can produce RF output power on the order of 10–12 W/mm of gate periphery [72], and should be useful through Ka-band, and potentially well into the millimeter-wave region, and potentially as high as 100 GHz. The RF power capability of these devices compares very favorably with the 1–1.5-W/mm RF power available from GaAS MESFETs and GaAs- and InP-based HEMTs.

VI. Summary and Conclusions

Starting from the early work in the 1930s to fabricate a solid-state equivalent of the vacuum triode, a variety of two-terminal diode and three-terminal transistor structures have been proposed and demonstrated. These devices have found practical application and have had a major impact upon the development of microwave and millimeter-wave systems. The development of high-performance solid-state devices has been closely linked to the availability of suitable semiconductor materials and related process technology. Since the performance of a solid-state device is dependent upon the electronic and physical parameters of the semiconductor material, there has been a continued investigation for new materials with improved parameters. This work started with early device demonstrations in Ge and quickly moved to Si, and then to GaAs, InP, and ternary III–V compounds such as AlGaAs and InGaAs, and heterostructures such as AlGaAs/GaAs and GaInAs/InP. The search for new materials is continuing and wide-bandgap semiconductors such as SiC, GaN, and the AlGaN/GaN heterostructure show promise for improved microwave and millimeter-wave device fabrication. The basic properties, power generation capabilities and state-of-the-art experimental results of a variety of two- and three-terminal solid-state devices have been presented. These solid-state devices have provided active sources for use as oscillators and amplifiers from UHF to terahertz frequencies. New materials such as GaN and SiC have the potential of increasing the power output significantly and ultimately vacuum-based ballistic devices may be used for generation of significant power levels at terahertz frequencies.

Acknowledgment

The authors would like to thank Dr. H. Eisele for his significant contributions to Section III.

References

[1] F. Braun, "Uber die Stromleitung durch Schwefelmetalle," *Ann. Phys. Chem.*, vol. 153, p. 556, 1874.
[2] J. Bardeen and W. H. Brattain, "The transistor, a semiconductor triode," *Phys. Rev.*, vol. 71, p. 230, 1948.
[3] W. Shockly, "The theory of p–n junction in semiconductors and p–n junction transistors," *Bell Syst. Tech. J.*, vol. 28, p. 435, 1949.
[4] J. E. Lilienfeld, "Method and apparatus for controlling electric currents," U.S. Patent 1 745 175, 1930.
[5] ——, "Device for controlling electric current," U.S. Patent 1 900 018, 1933.
[6] O. M. Stuetzer, "A crystal amplifier with high input impedance," *Proc. IRE*, vol. 38, p. 868, Aug. 1950.
[7] ——, "Junction fieldistors," *Proc. IRE*, vol. 40, pp. 1377–1381, Nov. 1952.
[8] W. Shockley, "A unipolar 'field-effect' transistor," *Proc. IRE*, vol. 40, p. 1365, Nov. 1952.
[9] ——, "Negative resistance arising from transit time in semiconductor diodes," *Bell Syst. Tech. J.*, vol. 33, pp. 799–826, July 1954.
[10] W. J. Read, "A proposed high frequency negative resistance diode," *Bell Syst. Tech. J.*, vol. 37, pp. 401–446, Mar. 1958.
[11] C. A. Lee, R. L. Batdorf, W. Wiegmann, and G. Kaminsky, "The read diode—An avalanching transit-time, negative-resistance oscillator," *Appl. Phys. Lett.*, vol. 6, pp. 89–91, Mar. 1965.
[12] R. L. Johnston, B. C. Deloach, and B. G. Cohen, "A silicon diode microwave oscillator," *Bell Syst. Tech. J.*, vol. 44, pp. 369–372, Feb. 1965.
[13] *IEEE Trans. Microwave Theory Tech. (Special Issue)*, vol. MTT-27, May 1979.
[14] J. B. Gunn, "Microwave oscillation of current in III–V semiconductors," *Solid State Comm.*, vol. 1, p. 88, 1963.
[15] B. K. Ridley and T. B. Watkins, "The possibility of negative resistance effects in semiconductors," *Proc. Phys. Soc. Lond.*, vol. 78, p. 293, 1961.
[16] C. Hilsum, "Transferred electron amplifiers and oscillators," *Proc. IRE*, vol. 50, pp. 185–189, Feb. 1962.
[17] H. D. Rees and K. W. Gray, "Indium phosphide: A semiconductor for microwave devices," *Solid State Electron.*, vol. 1, p. 1, 1976.
[18] L. Esaki, "New phenomenon in narrow germanium p-n junctions," *Phys. Rev.*, vol. 109, p. 603, 1958.
[19] S. M. Sze, *Physics of Semiconductor Devices*, 2nd ed. New York: Wiley, 1981.
[20] L. L. Chang, L. Esaki, and R. Tsu, "Resonant tunneling in semiconductor doublebarriers," *Appl. Phys. Lett.*, vol. 24, p. 593, 1974.
[21] J. Nishizawa, T. Ohmi, and T. Sakai, "Millimeter-wave oscillations from TUNNETT diodes," in *Proc. Eur. Microwave Conf.*, Paris, France, Sept. 1974, pp. 449–453.
[22] H. W. Rüegg, "A proposed punch-through negative-resistance diode," *IEEE Trans. Electron Devices*, vol. ED-15, pp. 577–585, Aug. 1968.

[23] S. M. Sze, D. J. Coleman, Jr., and A. Loya, "Current transport in metal–semiconductor–metal (MSM) structures," *Solid State Electron.*, vol. 14, pp. 1209–1218, 1971.
[24] H. Eisele and G. Haddad, "Active microwave diodes," in *Modern Semiconductor Device Physics*, S. M. Sze, Ed. New York: Wiley, 1998, ch. 6.
[25] E. R. Brown, W. D. Goodhue, T. C. L. G. Sollner, and C. D. Parker, "Fundamental oscillations up to 200 GHz in resonant tunneling diodes and new estimates of their maximum oscillation frequency from stationary-state tunneling theory," *J. Appl. Phys.*, vol. 64, p. 1519, 1988.
[26] R. K. Mains and G. I. Haddad, "Time-dependent modeling of resonant-tunneling diodes form direct solution of the Schrödinger equation," *J. Appl. Phys.*, vol. 64, p. 7, 3564, 1988.
[27] A. Rydberg, H. Grönquist, and E. Kollberg, "A theoretical and experimental investigation on millimeter-wave quantum well oscillators," *Microwave Opt. Technol. Lett.*, vol. 1, p. 333, 1988.
[28] E. R. Brown, T. C. L. G. Sollner, C. D. Parker, W. D. Goodhue, and C. L. Chen, "Oscillations up to 420 GHz in GaAs/AlAs resonant tunneling diodes," *Appl. Phys. Lett.*, vol. 55, p. 1777, 1989.
[29] E. R. Brown, J. R. Söderström, C. D. Parker, L. J. Mahoney, K. M. Molvar, and T. C. McGill, "Oscillations up to 712 GHz in nAs/AlSb resonant tunneling diodes," *Appl. Phys. Lett.*, vol. 58, p. 2291, 1991.
[30] M. E. Hines, "High frequency negative-resistance circuit principles for Esaki diode applications," *Bell Syst. Tech. J.*, vol. 39, p. 477, 1960.
[31] C. Kidner, I. Mehdi, J. East, and G. Haddad, "Power and stability limitations of resonant tunneling diodes," *IEEE Trans. Microwave Theory Tech.*, vol. 38, pp. 864–873, July 1990.
[32] J. B. Gunn, "Instabilities of current in III–V semiconductors," *IBM J. Res. Develop.*, vol. 8, p. 141, 1964.
[33] B. K. Ridley and T. B. Watkins, "The possibility of negative resistance effects in semiconductors," *Proc. Phys. Soc. Lond.*, vol. 78, p. 293, 1961.
[34] J. A. Copeland, "LSA oscillator-diode theory," *J. Appl. Phys.*, vol. 38, p. 3096, 1967.
[35] H. Eisele and G. Haddad, "High-performance InP Gunn devices for fundamental mode operation in D-band (110–170 GHz)," *IEEE Microwave Guided Wave Lett.*, vol. MGWL-5, p. 385, Nov. 1995.
[36] V. P. Kesan, D. P. Neikirk, B. G. Streetman, and P. A. Blaky, "A new transit-time device using quantum well injection," *IEEE Electron Dev. Lett.*, vol. EDL-8, p. 129, Apr. 1987.
[37] M. Elta and G. Haddad, "High-frequency limitations of IMPATT, MITATT, and TUNNETT mode devices," *IEEE Trans. Microwave Theory Tech.*, vol. MTT-27, pp. 442–449, May 1979.
[38] ——, "Large-signal performance of microwave transit-time devices in mixed tunneling and avalanche breakdown," *IEEE Trans. Electron Devices*, vol. ED-26, pp. 941–948, June 1979.
[39] P. T. Greiling, W. E. Schroder, and G. Haddad, "Basic principles and properties of avalanche transit-time devices," *IEEE Trans. Microwave Theory and Tech.*, vol. MTT-18, pp. 752–772, Nov. 1970.
[40] R. K. Mains, M. A. El-Gabaly, J. P. Sun, and G. Haddad, "Comparison of theoretical and experimental results for millimeter-wave GaAs IMPATTs," *IEEE Trans. Electron Devices*, vol. ED-31, pp. 1342–1352, Aug. 1984.
[41] J. East, C. Kidner, and G. Haddad, "Tunnel transit-time (TUNNETT) devices for terahertz sources," *Microwave Opt. Technol. Lett.*, vol. 4, p. 30, 1991.
[42] S. P. Kwok and G. I. Haddad, "Power limitations in BARITT devices," *Solid State Electron.*, vol. 19, pp. 795–807, 1976.
[43] J. East, H. Nguyen-Ba, and G. Haddad, "Design fabrication, and evaluation of BARITT devices for Doppler system applications," *IEEE Trans. Microwave Theory Tech.*, vol. MTT-24, pp. 943–948, Dec. 1976.
[44] H. Nguyen-Ba and G. Haddad, "Effects of doping profile on the performance of BARITT devices," *IEEE Trans. Electron Devices*, vol. ED-24, pp. 1154–1163, Sept. 1977.
[45] I. Mehdi, R. Mains, and G. Haddad, "Microwave and millimeter-wave power generation in silicon carbide avalanche devices," *J. Appl. Phys.*, vol. 64, pp. 3564–3569, 1988.
[46] J. East and G. Haddad, "Ballastic tunneling transit time devices for THz power generation," presented at the 12th Int. Space Terahertz Technol. Conf., San Diego, CA, Feb. 2001.
[47] H. Kroemer, "Theory of a wide-gap emitter for transistors," *Proc. IRE*, vol. 45, pp. 1535–1537, Nov. 1957.
[48] W. P. Dumke, J. M. Woodall, and V. L. Rideout, "GaAs–GaAlAs heterojunction transistor for high frequency operation," *Solid State Electron.*, vol. 15, pp. 1339–1334, Dec. 1972.
[49] M. Konagai, K. Katsukawa, and K. Takahashi, "(GaAl)As/GaAs heterojunction phototransistors with high current gain," *J. Appl. Phys.*, vol. 48, pp. 4389–4394, Oct. 1977.
[50] P. M. Asbeck, D. L. Miller, W. C. Petersen, and C. G. Kirkpatrick, "GaAs/GaAlAs heterojunction bipolar transistors with cutoff frequencies above 10 GHz," *IEEE Electron Device Lett.*, vol. EDL-3, pp. 366–368, Dec. 1982.
[51] S. L. Su *et al.*, "Double heterojunction AlGaAs/GaAs bipolar transistors by MBE with a current gain of 1650," *IEEE Electron Device Lett.*, vol. EDL-4, pp. 130–132, May 1983.
[52] R. J. Malik, J. R. Hayes, F. Capasso, K. Alavi, and A. Y. Cho, "High-gain AlInAs/GaInAs transistors grown by molecular beam epitaxy," *IEEE Electron Device Lett.*, vol. EDL-4, pp. 383–386, Apr. 1983.
[53] J. I. Song, W. P. Hong, C. J. Palmstrom, B. P. Van der Gaar, and K. B. Chough, "Millimeter-wave InP/InGaAs heterojunction bipolar transistors with a subpicosecond extrinsic delay time," *Electron. Lett.*, pp. 456–457, Mar. 1994.
[54] M. J. Rodwell *et al.*, "Submicron scaling of HBT's," *IEEE Trans. Electron Devices*, vol. 48, pp. 2606–2624, Nov. 2001.
[55] S. S. Iyer, G. L. Patton, S. S. Delage, S. Tiwari, and J. M. C. Stork, "Silicon–germanium base heterojunction bipolar transistors by molecular beam epitaxy," in *IEEE Int. Electron Device Meeting Dig.*, 1987, pp. 74–76.
[56] R. L. Pritchard, J. B. Angell, R. B. Adler, J. M. Early, and W. M. Webster, "Transistor internal parameters for small-signal representation," *Proc. IRE*, vol. 49, pp. 725–738, Apr. 1961.
[57] H. F. Cooke, "Microwave transistors: Theory and design," *Proc. IEEE*, vol. 59, pp. 1163–1181, Aug. 1971.
[58] T. H. Ning, "History and future perspective of the modern silicon bipolar transistor," *IEEE Trans. Electron Devices*, vol. 48, pp. 2485–2491, Nov. 2001.
[59] S. Middelhoek, "Projection masking, thin photoresist layers and interface effects," *IBM J. Res. Develop.*, vol. 14, pp. 117–124, Mar. 1970.
[60] P. Wolf, "Microwave properties of Schottky-barrier field-effect transistors," *IBM J. Res. Develop.*, vol. 14, pp. 125–141, Mar. 1970.
[61] K. Drangeid, R. Sommerhalder, and W. Walter, "High-speed gallium–arsenide Schottky barrier field-effect transistors," *Electron. Lett.*, vol. 6, pp. 228–229, Apr. 1970.
[62] J. Turner, A. Waller, R. Bennett, and D. Parker, "An electron beam fabricated GaAs microwave field-effect transistor," in *GaAs Related Compounds Symp.*, London, U.K., 1971, pp. 234–239.
[63] W. Baechtold, W. Walter, and P. Wolf, "X and Ku band GaAs MESFET," *Electron. Lett.*, vol. 8, pp. 35–37, Jan. 1972.
[64] M. Fukuta, T. Mimura, I. Tujimura, and A. Furumoto, "Mesh source type microwave power FET," in *Int. Solid-State Circuits Conf. Tech. Dig.*, 1973, pp. 84–85.
[65] L. Napoli *et al.*, "High power GaAs FET amplifier—A multi-gate structure," in *Int. Solid-State Circuits Conf. Tech. Dig.*, 1973, pp. 82–83.
[66] M. Driver, M. Geisler, D. Barrett, and H. Kim, "S-band microwave power FET," in *IEEE Int. Electron Device Meeting Dig.*, 1973, pp. 393–395.
[67] L. Esaki and R. Tsu, "Superlattice and negative conductivity in semiconductors," IBM, Yorktown Heights, NY, IBM Res. Rep. RC-2418, 1969.
[68] H. L. Stormer, R. Dingle, A. C. Gossard, W. Wiegmann, and M. D. Sturge, "Two-dimensional electron gas at differentially doped GaAs–AlGaAs heterojunction interface," *J. Vac. Sci. Technol.*, vol. 16, pp. 1517–1519, 1979.
[69] T. Mimura, S. Hiyamizuk, T. Fujii, and K. Nanbu, "A new field effect transistor with selectively doped GaAs/n–AlGaAs heterostructures," *Jpn. J. Appl. Phys.*, vol. 19, pp. L225–L227, 1980.
[70] H. Fukui, "Determination of the basic device parameters of a GaAs MESFET," *Bell Syst. Tech. J.*, vol. 58, pp. 771–797, Mar. 1979.
[71] R. J. Trew, "SiC microwave devices," in *SiC Materials and Devices*, Y. S. Park, Ed. New York: Academic, 1998, vol. 52, ch. 6, pp. 237–282.
[72] R. J. Trew, "Wide bandgap semiconductor transistors for microwave power amplifiers," *IEEE Microwave Mag.*, vol. 1, pp. 46–54, Mar. 2000.

George I. Haddad (S'57–M'61–SM'66–F'72–LF'97) received the B.S.E., M.S.E., and Ph.D. degrees in electrical engineering from The University of Michigan at Ann Arbor.

He is currently the Robert J. Hiller Professor of Electrical Engineering and Computer Science at the University of Michigan at Ann Arbor, and was Chair of the Department (1975–1986, 1991–1997). He also served as Director of the Electron Physics Laboratory (1969–1975), Director of the Solid-State Electronics Laboratory (1986–1991), and Director of the Center for High Frequency Microelectronics (1986–2000). His expertise is in the areas of microwave and millimeter-wave devices and integrated circuits, microwave-optical interactions, opto-electronic devices, and integrated circuits.

Dr. Haddad is a member of Eta Kappa Nu, Sigma Xi, Phi Kappa Phi, Tau Beta Pi, the American Society for Engineering Education, and the American Physical Society. He is also a member of the National Academy of Engineering. He was editor-in-chief of the IEEE TRANSACTIONS ON MICROWAVE THEORY AND TECHNIQUES (1968–1971) and was a member of the IEEE Microwave Theory and Techniques Society (IEEE MTT-S) Administrative Committee (1970–1976). He has also served and participated on numerous other IEEE committees and activities. He was the recipient of the Curtis W. McGraw Research Award of the American Society for Engineering Education (1970), The College of Engineering Excellence in Research Award (1985), the Distinguished Faculty Achievement Award (1986) of The University of Michigan at Ann Arbor, and the S. S. Attwood Award of the College of Engineering. He was also the recipient of the IEEE MTT-S Distinguished Service Award and the IEEE MTT-S Distinguished Educator Award (1996).

Robert J. Trew (S'71–M'74–SM'87–F'91) received the Ph.D. degree from the University of Michigan at Ann Arbor, in 1975.

He is currently the Willis G. Worcester Professor of Engineering and Head of the Electrical and Computer Engineering Department of the Virginia Polytechnic Institute and State University, Blacksburg. From 1997 to 2001, he was Director of Research for the U.S. Department of Defense (DoD), with management oversight responsibility for the $1.3 billion yearly basic research programs of the DoD. He was Vice-Chair of the U.S. Government interagency committee that planned and implemented the U.S. National Nanotechnology Initiative. From 1992 to 1997, he served as a Program Manager in the Electronics Division of the Army Research Office. His academic career includes 17 years with North Carolina State University, and four years as the George S. Dively Distinguished Professor of Engineering and Chair of the Electrical Engineering and Applied Physics Department, Case Western Reserve University. He has authored or co-authored over 140 publications, 14 book chapters, and has given over 280 technical and programmatic presentations. He holds four patents.

Dr. Trew is a member of the Materials Research Society, the Electromagnetics Academy, the American Association for the Advancement of Science (AAAS), the American Society for Engineering Education (ASEE), Sigma Xi, Eta Kappa Nu, and Tau Beta Pi. He serves on the IEEE Microwave Theory and Techniques Society (IEEE MTT-S) Administration Committee. He was editor-in-chief of the IEEE TRANSACTIONS ON MICROWAVE THEORY AND TECHNIQUES (1995–1997), and is currently inaugural co-editor of the *IEEE Microwave Magazine*. He is also a member of the Editorial Board of the PROCEEDINGS OF THE IEEE. He was an IEEE Microwave Distinguished Lecturer (1997–2000). He was the recipient of an IEEE Third Millennium Medal Award, the 1998 IEEE MTT-S Distinguished Educator Award, the 1991 Alcoa Foundation Distinguished Engineering Research Award, and a 1992 Distinguished Scholarly Achievement Award from North Carolina State University.